polysaccharides

MDPI

Review

Polysaccharide Bioinks for 3D Bioprinting: A Guide to Translation

Adrian Bibis [1], Alexandru Paraschiv [1], Nicolae Dan Batalu [2], Anita Ioana Visan [3,*] and Rodica Cristescu [3,4,*]

[1] National Research and Development Institute for Gas Turbines COMOTI, Bd. Iuliu Maniu 220D, 061126 Bucharest, Romania; adrian.bibis@comoti.ro (A.B.); alexandru.paraschiv@comoti.ro (A.P.)
[2] Department of Metallic Materials Science, Physical Metallurgy, Faculty of Materials Science and Engineering, National University of Science and Technology POLITEHNICA Bucharest, Splaiul Independenței 313, 060042 Bucharest, Romania; dan.batalu@upb.ro
[3] Lasers Department, National Institute for Laser, Plasma and Radiation Physics, 409 Atomistilor Street, 077125 Magurele, Romania
[4] Research Institute of the University of Bucharest—ICUB, University of Bucharest, 050663 Bucharest, Romania
* Correspondence: anita.visan@inflpr.ro (A.I.V.); rodica.cristescu@inflpr.ro (R.C.)

Abstract

Polysaccharide-based hydrogels offer versatile platforms for three-dimensional bioprinting, but translation requires coordinated assessment of formulation, processing, and biological performance. This narrative review connects backbone chemistry and functionalization with rheology, crosslinking, printing modality, cellular responses, and manufacturing requirements. It examines alginate, hyaluronic acid, chitosan, cellulose derivatives, gellan gum, and complementary polysaccharides, distinguishing cell-laden bioinks from acellular biomaterial inks and supporting materials. A study-specific framework separates material feasibility, cell-laden printing, functional in vitro outcomes, preclinical evaluation, and preliminary human feasibility without assigning maturity scores to entire material families. Print fidelity and cellular remodeling impose competing requirements whose balance is formulation- and application-dependent. Dual or sequential crosslinking, dynamic networks, and support-bath printing provide complementary approaches rather than a universal solution. Inconsistent reporting limits cross-study comparison; a minimum reporting set is therefore proposed. Sterilization, raw-material variability, quality control, long-term safety, and regulatory classification are considered alongside formulation design. Future priorities include tissue-appropriate viscoelasticity, granular architectures, hierarchical vascularization, and reproducible data-driven optimization. Clinical translation will require stronger links between manufacturing reproducibility and sustained biological function, rather than printing accuracy alone.

Keywords: 3D bioprinting; polysaccharide hydrogel; alginate; hyaluronic acid; nanocellulose; gellan gum; crosslinking; rheology; tissue engineering; translational readiness

Check for updates

Academic Editors: Tina Maver and Uroš Maver

Received: 4 September 2026
Revised: 2 October 2026
Accepted: 9 October 2026
Published: 28 October 2026

Copyright: © 2026 by the authors. Licensee MDPI, Basel, Switzerland. This article is an open access article distributed under the terms and conditions of the Creative Commons Attribution (CC BY) license.

1. Introduction and Review Scope

1.1. The Bioink Challenge

Conventional tissue engineering combines a preformed porous scaffold with post hoc cell seeding [1]. Although this approach can reproduce bulk geometry, it seldom recreates the zonal cell distributions, graded matrix composition, and embedded vascular hierarchy's characteristic of native tissue. Three-dimensional (3D) bioprinting recasts the task as spatially programmed deposition: computer-aided model direct cells, hydrogel precursors, and signaling molecules to defined locations, such that composition and architecture are specified together during fabrication [1]. Two distinctions from the biofabrication literature help

to appropriately bound this ambition. First, a bioink contains living cells during processing, unlike a biomaterial ink that is printed without cells, whether or not it is seeded afterwards; this distinction is consequential because it defines the permissible processing window [2]. Second, geometric fidelity is necessary but not sufficient. Functional maturation remains the field's central shortfall, and gains in printing accuracy have outpaced the biological performance of printed constructs by a considerable margin [3]. The ink itself sits at the center of this problem. A printable hydrogel must pass through a nozzle or cure within an optical field and then solidify rapidly enough to retain a filament or voxel, while supporting a cell population whose survival, adhesion, and phenotype depend on hydration, ligand presentation, mesh size, stiffness, and viscoelastic relaxation. Those requirements overlap only partly. The biofabrication window formalizes the resulting tension: formulations that achieve high fidelity commonly rely on higher polymer concentrations or denser crosslinking, both of which tend to constrain cell spreading, migration, and matrix remodeling [4]. The design question, then, is not simply how to balance one axis against the other, but how to decouple them wherever the chemistry permits.

Throughout this review, 'bioink' denotes a formulation containing living cells during printing, whereas 'biomaterial ink' denotes a formulation printed without cells, irrespective of subsequent cell seeding [2]. A supporting or sacrificial material is identified by its processing role and is not automatically a bioink. Injectable or cast hydrogels are discussed as mechanistic or formulation precedents unless printing is demonstrated. Where a cited article uses broader terminology in its title, the original title is retained in the bibliography, but the discussion follows the experimental distinction.

1.2. Polysaccharide Bioink Design

Polysaccharides hold a privileged place in this design space for four reasons. They are strongly hydrophilic, forming high-water-content networks at low polymer concentrations; their hydroxyl, carboxyl, and amine substituents offer established chemical handles for grafting adhesive peptides, methacryloyl groups, phenols, norbornenes, and other reactive functionalities; several form gels through mild physical mechanisms—ionic bridging, thermoreversible helix formation, and hydrophobic association—that require neither radicals nor organic solvents; and some convey genuine biological information. Hyaluronic acid (HA), for example, is an endogenous glycosaminoglycan that engages CD44 and related receptors [5]. Alginate illustrates the corresponding limitation. Its gelation is rapid, inexpensive, and cytocompatible, but the polymer supplies neither integrin ligands nor mammalian-enzyme-cleavable bonds [6,7]. Polysaccharide bioink design is therefore seldom a matter of selecting a single polymer; it is the deliberate composition of a network containing a structural component, a bioactive component, and a stabilization chemistry.

Three class-wide limitations recur throughout this review. First, apart from the partial exception of HA and chondroitin sulfate, polysaccharides are not generally recognized by mammalian cell-surface receptors; adhesion must therefore be engineered rather than presumed [7,8]. Second, mammalian enzymes cleave few polysaccharide backbones, meaning that degradation requires chemical design—through hydrolytically labile linkages, protease-sensitive peptide crosslinks, or, where appropriate, acceptance of persistence and assessment as a permanent implant [9–11]. Third, these are natural products, with molecular weight and degree of substitution varying by batch and source; consequently, formulation parameters cannot be transferred between suppliers without re-characterization [12,13]. Together, these features—not any isolated failure of printability—define the realistic limits of current polysaccharide-bioink performance.

Their continued use also reflects manufacturability. Alginate, HA, gellan gum, chitosan, carrageenan, and pullulan are produced industrially for food, cosmetic, and pharmaceutical

applications, while specification frameworks for medical-grade alginate and chitosan raw materials have been available for more than two decades [13]. Purification routes that yield endotoxin-controlled, implantation-grade alginate were established for immunoisolation microcapsules and remain a useful reference point for clinical-grade polysaccharide sourcing [14]. Few synthetic bioink chemistries yet offer comparable supply-chain maturity. That maturity represents a genuine translational asset.

1.3. What This Review Adds

This review organizes polysaccharide bioink development around the relationships among backbone chemistry, functionalization, rheology, crosslinking, printing modality, biological performance, and manufacturing constraints. Its emphasis is on three complementary aspects: formulation–process–function relationships, study-specific interpretation of experimental evidence, and the incorporation of translational requirements into material design. Related reviews provide material- and process-focused context [15–17]. First, the review follows a single design chain rather than a material catalogue. Backbone chemistry and substitution determine rheology and the available crosslinking options; these delimit feasible printing modalities; modality and crosslinking dose define the mechanical and chemical environment presented to cells; and that environment ultimately shapes tissue function and the quality attributes a manufactured construct must meet. This sequence makes the coupling between formulation decisions and downstream translational constraints more apparent than a polymer-by-polymer treatment generally can.

Second, the framework in Section 1.5 distinguishes material feasibility, cell-laden printing, functional in vitro validation, preclinical evaluation, and preliminary human feasibility. Evidence is attributed to a defined formulation and endpoint rather than assigned as a maturity grade to a material family. A dedicated summary table separately identifies experimental, methodological, and regulatory sources.

Third, manufacturing, sterilization, and regulatory classification are considered formulation variables that feed back into chemistry and rheology, rather than being relegated to a compliance appendix. The synthetic translational-barriers table from Section 8.6 renders that feedback operational by linking each principal barrier to its root cause and to published, cited solutions. Together, these perspectives provide a framework for interpreting why a formulation performs under a defined set of conditions and which validation steps remain before its intended application can be considered.

1.4. Literature Search Strategy and Inclusion Criteria

This is a narrative comprehensive review rather than a systematic review, and its coverage should accordingly be understood as expert-curated. Literature was identified through iterative searching of PubMed/MEDLINE, Web of Science Core Collection, and Scopus. Publisher databases—MDPI, Elsevier ScienceDirect, Wiley Online Library, ACS Publications, Springer Nature, Royal Society of Chemistry, and Frontiers—were used for full-text retrieval, while regulatory-agency, legislative, and standards databases supplied primary compliance sources.

Query sets followed the same design chain used to organize the review: material-level (“alginate bioink”, “hyaluronic acid bioink”, “nanocellulose bioprinting”, “gellan gum bioink”, “chitosan bioink” and related terms for chondroitin sulfate, dextran, carrageenan, pectin, pullulan, starch, and agarose); chemistry-level (“methacrylation”, “click chemistry hydrogel”, “dynamic covalent bioink”, “enzymatic crosslinking bioink”, “photocrosslinking bioink”); modality-level (“extrusion bioprinting”, “FRESH bioprinting”, “volumetric bioprinting”, “DLP bioprinting”, “digital light processing bioink”); tissue-level (cartilage, bone, skin, vascular, cardiac, neural, hepatic, tumor model); and translational-level (“bioink ster-

ilization", "bioprinting regulatory", "advanced therapy medicinal product", "bioprinting critical quality attributes").

The temporal window gave priority to peer-reviewed work published between 2014 and 2026, the period associated with the modern biofabrication-window and bioink-definition literature. Earlier foundational primary reports were retained when they established concepts still used in current formulation design, including ligand-functionalized alginate [7] and partial oxidation as a route to alginate degradation [9]. Foundational reviews were included separately for conceptual context [1,4]. Records were included if they (i) reported original work on cell-laden polysaccharide bioinks or acellular polysaccharide biomaterial inks relevant to biofabrication with quantitative rheological, mechanical, printability, or biological data, or (ii) constituted a peer-reviewed review, standard, or agency-guidance document providing synthesis-level information unavailable in the primary literature. Exclusion criteria were conference abstracts lacking a peer-reviewed full paper; preprints not subsequently peer-reviewed; non-cell-laden 3D printing of bulk hydrogel scaffolds without a bioprinting context; and papers in which the polysaccharide component was ancillary rather than structural to the bioink. Each retained bibliographic record was checked against the indexing record and the publisher digital object identifier.

The evidence tables are intended to illustrate formulation–process–outcome relationships. Primary experimental studies provide the basis for formulation-specific performance statements, whereas reviews, nonprinted hydrogel studies, standards, and agency documents provide mechanistic or contextual support. A source contributes to a direct bioink-performance claim only when the relevant formulation, printing route, cellular status, and measured endpoint are identifiable. Information not reported in the source is not inferred from a related formulation or from another study in the same material family.

For each table entry, interpretation distinguishes the structural polysaccharide and its modification, the role of other components, whether living cells are present during printing, the experimental setting, the endpoint, and the observation period where reported. Particular attention is given to studies that connect a defined formulation change to a measured processing or biological outcome. Multiple reports addressing the same mechanism provide context but do not constitute independent replication unless their experimental conditions and endpoints are sufficiently comparable. Selected examples of this attribution are provided in Table A1.

The selection is purposive and not exhaustive. Consequently, expressions such as 'preclinical evidence' describe the experiments available in the cited studies, not the prevalence of an evidence level across the entire literature. No pooled effect sizes, comparative efficacy ranking, formal certainty grades, or quantitative estimates of clinical readiness are derived from these tables.

1.5. Evidence Framework and Interpretation

This narrative review uses an author-defined, five-level framework to distinguish the type of validation available for a specific formulation and application. The framework is a descriptive aid, not a validated risk-of-bias instrument, a formal certainty-of-evidence assessment, or a technology-readiness score. Technical feasibility, biological performance, independent replication, and clinical readiness are related but distinct attributes.

Level 1: Material or fabrication feasibility. The relevant chemistry, rheology, crosslinking, or printing behavior has been demonstrated, but survival of cells incorporated during printing has not been established. Acellular printing and extract-based cytocompatibility assays belong to this level when used to support a printing claim.

Level 2: Cell-laden printing with basic biological compatibility. Living cells are present during printing, and post-printing survival or basic cellular compatibility is demonstrated. Viability alone does not establish tissue-specific function.

Level 3: Functional in vitro validation of a cell-laden printed construct. In addition to post-printing compatibility, the study reports an application-relevant biological endpoint, such as differentiation, matrix deposition, metabolic activity, or a reproducible drug response. The endpoint and observation period must be stated; no universal culture-duration threshold is imposed.

Level 4: Preclinical in vivo evaluation of a printed construct. A defined printed formulation is evaluated in an animal model with application-relevant outcomes. The animal model, implantation site, controls, and follow-up determine the scope of the inference. Ectopic tissue formation does not establish restoration of function at the intended anatomical site.

Level 5: Preliminary human feasibility. A defined printed formulation has been used in humans and its outcomes reported in a peer-reviewed study. Clinical feasibility is not equivalent to comparative efficacy, regulatory approval, or routine clinical use. Human cells used in culture or implanted into animals do not constitute Level 5 evidence.

The biological status of the printed material is recorded separately as cell-laden during printing, printed without cells and subsequently seeded, or acellular. A nonprinted hydrogel study is identified as mechanistic supporting evidence rather than assigned a printing level. Similarly, support baths, sacrificial materials, and studies using non-polysaccharide matrices can inform process design without establishing the performance of a polysaccharide bioink.

Level assignment is restricted to the experiment and endpoint reported in the cited study. Where the information required for a higher level is absent or ambiguous, the lower directly supported level is retained or the classification is left unassigned. Multiple publications from the same laboratory do not by themselves establish independent replication. Replication is described only when independent groups investigate sufficiently comparable formulations, processing conditions, and endpoints.

When findings differ, formulation composition, molecular weight, substitution, cell population, printing conditions, crosslinking exposure, assay, and follow-up are considered before treating the studies as contradictory. Results obtained under different conditions are reported as context-dependent; unresolved disagreement is identified explicitly. No pooled effect or family-wide maturity score is calculated. Regulatory guidance and standards are classified by document type and jurisdiction, outside the five-level experimental framework.

2. Principles of Bioink Design and Printing Modalities

2.1. Performance Requirements Are Set by the Modality, Not by the Polymer

The most frequent formulation error is to optimize a polysaccharide ink in the abstract. Printability is not an intrinsic material property, but rather a compatibility between a material and a particular deposition process, with permissible viscosity, gelation kinetics, optical properties, and cell density varying by orders of magnitude across modalities [1,16]. Design should begin with the modality and work backwards to chemistry.

These differences are quantitative, and they matter. Extrusion accepts viscous, yield-stress inks and high cell densities, but its features are limited by the nozzle and by spreading of the emerging filament; droplet methods place small volumes with precision but demand low-viscosity fluids; light-based methods separate resolution from ink viscosity but require photochemistry, optical clarity, and controlled attenuation; and volumetric methods dispense with layer-wise deposition entirely, at the cost of a resin whose refractive index and absorbance must be engineered around the cell payload [1,18–20]. A polysaccharide formulation tuned for one such envelope will usually be unsuitable for another. Reports that designate a formulation simply "printable" without specifying modality, nozzle, temperature, and crosslinking sequence are consequently difficult to reproduce; the corresponding reporting requirements are consolidated in Section 6.3.

2.2. Extrusion-Based Printing

Extrusion dominates polysaccharide bioprinting because it accommodates a broad viscosity range, high cell densities, and yield-stress fluids, and is compatible with the physical gelation mechanisms that most polysaccharides provide natively. The mechanical cost is substantial. As cells traverse a converging nozzle, they encounter shear stresses that rise with flow rate and fall with nozzle radius; mechanical exposure can affect viability and later cellular behavior, creating a trade-off with the resolution offered by finer nozzles [21–23]. Shear history is not invariably harmful. In oxidized alginate–gelatin inks, extrusion-imposed shear has been deliberately used to align C2C12 myoblasts along the filament axis and promote later myogenic differentiation, indicating that the shear field is a design variable, not solely a hazard [24]. Recent syntheses of damage mechanisms across modalities distinguish shear-induced membrane injury from crosslinking-associated and osmotic insults, while cataloguing mitigation strategies including nozzle-geometry optimization, shear-thinning additives, and post-print recovery protocols [21]. Computational fluid dynamics makes the coupling both explicit and quantitative: nozzle diameter and taper, applied pressure, and print speed can be mapped onto wall shear stress and residence-time distributions, turning an empirical parameter sweep into a calculable mechanical dose reportable alongside viability [22].

The magnitude of this coupling is illustrated by gelatin–alginate bioinks containing 1% *w*/*v* alginate and 5–10% *w*/*v* gelatin. Ouyang et al. reported that the complex viscosity at the gelation point increased from 0.57 ± 0.04 to 1.84 ± 0.16 Pa·s as gelatin concentration increased from 5% to 10% [23]. These values were obtained by oscillatory testing at 0.1% strain and 1.5 Hz, with the gelation point defined by the crossover of the storage and loss moduli; they are not steady-shear viscosities at a specified nozzle shear rate [23]. The study examined printing temperatures of 22.5–30 °C and showed that temperature and holding time jointly altered gelation, extrusion behavior, and survival of encapsulated mouse embryonic stem cells [23].

For that particular cell–material–process combination, estimated maximum shear stresses below 100 Pa were associated with viability above 90% [23]. This should be interpreted as a study-specific observation rather than a transferable damage threshold: cell type, exposure duration, nozzle geometry, and gelation state all affect the response. The numerical outcome also depends on when it is measured. For example, human chondrocytes printed in a nanocellulose–alginate bioink showed viabilities of 73% and 86% after 1 and 7 days of three-dimensional culture, respectively [25]. Consequently, rheological values and viability percentages are informative only when reported together with the formulation, measurement protocol, processing conditions, and assay time.

Two extrusion variants merit separate consideration because they alter what polysaccharides are required to do. In embedded or support-bath printing, filament is deposited

into a yield-stress medium that supplies transient mechanical support and thereby decouples shape retention from the ink's own rheology. The freeform reversible embedding of suspended hydrogels approach demonstrated this principle using a gelatin microparticle bath and was later extended to a full-size anatomical heart model, revealing both the geometric reach and the fidelity limits of the method [26,27]. In coaxial and triaxial extrusion, ink and crosslinker meet at the nozzle exit, or a sacrificial core is co-extruded; gelation can thus be rapid without sacrificing nozzle patency. This strategy has been applied to enzymatically crosslinkable HA–tyramine inks and multi-compartment bone constructs [28,29]. Embedded printing has since been systematized. Comparative design analyses specify a support bath with sufficient yield stress to retain the deposited filament, rapid self-healing behind the moving nozzle, and interfacial tension low enough to prevent filament breakup, while making clear that bath and ink must be matched rather than optimized in isolation [30,31]. Polysaccharides may serve as the bath as well as the ink: gellan gum granular suspension media have been characterized specifically as biofabrication support baths, with yield stress, recovery, and self-healing quantified. This permits very low-viscosity, cell-friendly inks to print at a fidelity that their intrinsic rheology cannot sustain [32]. Embedded printing coupled with sacrificial writing has also produced perfusable, physiologically graded organ models, suggesting that the approach is now a route to function rather than geometry alone [33].

2.3. Droplet-Based and Laser-Assisted Printing

Droplet-based printing places discrete volumes rather than continuous filaments, making droplet formation, landing, coalescence, and post-deposition stabilization central to formulation design. Nozzle-based dispensing must balance fluidity with sufficient polymer content to form a stable network after deposition, while cell aggregates and premature gelation can compromise delivery. The relevant operating window is therefore specific to the actuation method and formulation rather than defined by a single low-viscosity limit [1,16].

Microvalve-based printing illustrates the importance of treating actuation and cellular exposure together. Blaeser et al. used a fluid-dynamic description of the nozzle to relate controlled shear exposure to cell viability and proliferative potential [34]. This study provides a basis for analyzing mechanical dose, but its results should not be transferred directly to continuous extrusion or laser-assisted systems, which impose different stress histories.

Laser-assisted transfer avoids passage through a dispensing nozzle, but this does not remove all sources of cellular injury. In alginate systems, polymer concentration, laser fluence, droplet impact, and the subsequent calcium-mediated gelation step can each influence the outcome [35]. Gudapati et al. examined NIH-3T3 fibroblasts in alginate microspheres and compared gelation periods of 2 and 10 min [35]. After 24 h of incubation, the shorter treatment could provide a protective effect associated with the forming gel membrane, whereas the longer exposure reduced viability, which the authors associated with restricted nutrient and oxygen transport through a thicker membrane [35].

These examples show that droplet or jet generation and network formation should be optimized as separate but coupled operations. For polysaccharide formulations, a mild initial deposition step does not establish the compatibility of the completed process if subsequent crosslinking produces excessive exposure or transport limitation. Cell survival should therefore be assessed after the full printing and stabilization sequence, with the gelation conditions reported explicitly [16,34,35].

2.4. Light-Based and Volumetric Modalities

Light-based printing transfers much of the formulation constraint from filament stability to reaction kinetics and optical transport. In stereolithography and digital light processing, the material must form a spatially confined network at a controlled exposure while permitting replenishment of uncured precursor. Photoinitiator absorption, oxygen inhibition, light attenuation, scattering, and cell loading therefore require consideration alongside viscosity [18]. Functionalized polysaccharides can provide the reactive backbone, but printing a geometrically accurate hydrogel and maintaining living cells within it remain distinct validation steps.

Hyaluronic acid illustrates how reaction mechanism affects process performance. Steudter et al. compared thiol–ene and methacrylate formulations based on HA of the same molecular weight and comparable functionalization [36]. Thiol–ene precursors showed longer storage stability and faster photocrosslinking under the tested conditions; a 4% w/v HA formulation crosslinked with a dithiol enabled DLP fabrication of layers containing 100 µm holes within 2 s [36]. These results establish a chemistry–fabrication relationship rather than, by themselves, demonstrating the biological performance of a cell-laden printed construct.

Other polysaccharides show why this distinction matters. Norbornene-functionalized pullulan was formulated for DLP printing through thiol–ene crosslinking, with cytocompatibility evaluated separately by exposing L929 cells to hydrogel extracts [37]. This is an acellular biomaterial-ink demonstration, not evidence of cell survival during printing. In contrast, the study of methacrylated κ-carrageenan combined DLP fabrication across a 1–5% w/v material range with encapsulation experiments showing viability and proliferation of NIH-3T3 cells [38]. The biological result should be interpreted for the tested formulation rather than assumed to apply to every concentration in the fabrication series.

Volumetric printing further changes the design problem by exposing the resin to a sequence of projections that defines the construct in three dimensions rather than layer by layer [19]. Bernal et al. produced organoid-laden gelatin constructs at centimetre scale in less than 20 s and demonstrated liver-related metabolic activity after culture [20]. Because the matrix in that study is gelatin-based, the result is a benchmark for optical and architectural design, not direct validation of a polysaccharide resin. Its relevance lies in showing why cell-induced scattering and optical tuning must be considered explicitly when transferring volumetric methods to a new material.

For polysaccharide-based light printing, formulation comparisons should therefore separate photochemical conversion and geometric performance from post-printing biological outcomes. Faster curing or smaller features alone do not demonstrate a more permissive cellular microenvironment. The exposure and characterization information needed to interpret these results is summarized in Section 6.3.

2.5. Cell Payload as a Formulation Variable

Cell density is a material variable rather than a biological afterthought. Cells occupy volume, scatter light, alter effective viscosity, and may nucleate defects at high loading; conversely, biological performance across most tissue targets improves with density, and the highest-functioning printed constructs reported to date generally employ dense cellular or organoid payloads rather than sparse suspensions [20,39]. Printability envelopes measured using acellular inks therefore transfer only approximately to cell-laden formulations. Recharacterization at the intended cell density is a minimum expectation for a credible bioink report [16].

3. Chemistry and Structure–Property Relationships of Polysaccharides

3.1. Backbone Architecture, Charge and Molecular Weight

The behavior of polysaccharide inks is governed chiefly by four backbone descriptors. Charge comes first. In dilute salt, polyanions including alginate, HA, gellan gum, carrageenan, pectin and chondroitin sulfate expand through intramolecular electrostatic repulsion, respond strongly to ionic strength, and can be gelled with multivalent counterions; the polycation chitosan behaves in the opposite sense because protonation equilibria dominate, whereas neutral backbones—dextran, pullulan, agarose, starch and cellulose derivatives—are controlled principally by hydrogen bonding, hydrophobic association and chain entanglement [6,39,40]. Stereochemical regularity is the second descriptor. Ordered sequences promote cooperative junction formation and stiff, occasionally brittle, networks: the double helices of agarose, gellan and κ-carrageenan, together with cellulose crystalline domains, exemplify this behavior; irregular or extensively substituted sequences instead tend toward viscous solutions with weak structure [40,41].

Molecular weight and its distribution constitute the third descriptor, setting zero-shear viscosity, entanglement density and, for ionically gelled systems, the balance between elasticity and syneresis. A systematic study of a large alginate library showed that molecular weight and monomer composition, rather than nominal concentration alone, predict which grades are suitable for biofabrication; its screening protocol should therefore be treated as best practice before formulation development [12]. The fourth descriptor is substitution. Degree of acetylation in chitosan, degree of methyl esterification in pectin, sulfation pattern in chondroitin sulfate and carrageenan, and acyl content in gellan gum can each substantially shift solubility, gelation temperature and mechanics. Thus, "the same polysaccharide" purchased from two suppliers may not be the same material [39,41,42].

3.2. Functional-Group Handles and the Bioactivity Cost of Modification

Carboxyl groups permit carbodiimide-mediated amidation and hydrazide coupling; hydroxyls permit methacrylation, etherification and oxidation to aldehydes; amines permit Schiff-base and reductive-amination chemistry; and periodate oxidation transforms vicinal diols into dialdehydes, introducing hydrolytic lability while supplying imine-forming sites [9,43]. Yet every such modification perturbs a structure that may be biologically recognized. Systematic variation in HA modification chemistry and degree of substitution has shown a measurable decline in CD44 recognition as modification increases, so the covalent chemistry that renders HA printable can undermine the very bioactivity that justified its selection [8]. The broader principle is underappreciated: modification degree should be reported, minimized to that needed to meet the mechanical target, and accompanied by bioactivity measurements in the modified material rather than assumptions drawn from the parent polymer.

3.3. Blends, Interpenetrating Networks and Nanocomposites

No single polysaccharide reliably provides printability, degradability and adhesion at once; credible formulations are consequently usually multicomponent. Three architectures recur. Physical blends pair a rheology modifier with a bioactive or degradable partner, as in nanocellulose–alginate and nanofibrillated cellulose–gellan systems [25,43]. Interpenetrating and semi-interpenetrating networks place independent crosslinking chemistries in the same volume, exemplified by printable gellan–dextran methacrylate networks later functionalized with RGD peptides [44]. Nanocomposites distribute a rigid phase—cellulose nanocrystals, mineral or nanozyme particles—to increase yield stress or confer biological function without raising the soluble polymer fraction [45,46]. These strategies impose corresponding characterization duties: one must exclude phase separation and rigid-phase

filtration at the nozzle, while recognizing that reinforcement can be transient if one network dissolves more rapidly than the other. Two variants merit separate mention. In-line compounding dispenses with a pre-formulated blend: alginate, chitosan and kaolin have been homogeneously mixed within a portable print head, allowing otherwise incompatible components to meet only seconds before deposition [47]. Nor do interpenetrating networks require two covalent chemistries; host–guest supramolecular association superimposed on an alginate network has increased toughness and adhesion, both benchmarked against the single-network control [48].

Blends, interpenetrating networks, and nanocomposites distribute structural and biological functions among different components [25,43–46]. Their added complexity should be justified by a measurable advantage over an appropriate simpler formulation. Section 5 considers how the corresponding stabilization mechanisms can be selected and combined.

The chemical and physical modification strategies discussed in this section are summarized in Figure 1, providing an overview of routes used to adapt polysaccharides for biofabrication [49].

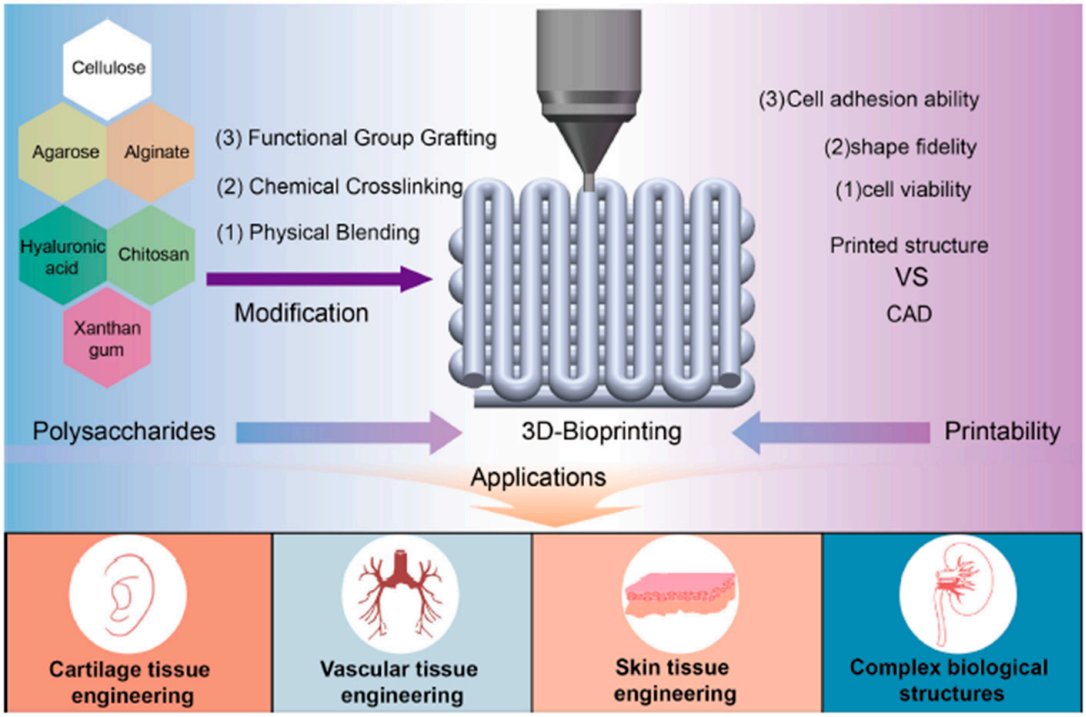

Figure 1. Overview of chemical and physical strategies used to modify polysaccharides for bioprinting and tissue-engineering applications. The scheme complements the discussion of functionalization and multicomponent design in Section 3. This figure was reproduced from [49], under CC BY.

4. Material-Specific Analysis of Polysaccharide Bioinks

The representative backbone structures summarized in Figure 2 provide a common basis for the material-specific discussion. The scheme identifies the constituent sugars, anomeric configurations, linkage positions, and principal ionizable or substitutable groups; native polysaccharides nevertheless vary in sequence distribution, branching, substitution, and molecular weight [6,17,39–41]. These variations are functionally important and should not be obscured by a single idealized repeat. The structures shown therefore serve as chemical reference motifs rather than specifications for every commercial grade.



Figure 2. Representative backbone structures of the twelve polysaccharide systems discussed in Section 4, shown in condensed glycosidic notation. Alginate contains mannuronate- and guluronate-rich blocks and mixed sequences; chitosan contains glucosamine and N-acetylglucosamine residues; cellulose derivatives retain the cellulose backbone but differ in hydroxyl substitution. Gellan acylation, chondroitin sulfate sulfation, and pectin esterification vary with material source and processing. Dextran branching is source-dependent; starch comprises predominantly linear amylose and branched amylopectin. The pectin panel shows the homogalacturonan domain, not the complete pectin architecture. For comparison, agarose contains 3,6-anhydro-L-galactose, whereas κ-carrageenan contains 3,6-anhydro-D-galactose. Counterions and printing-specific functionalization are omitted for clarity [6,17,39–41,50–52]. Original schematic, assembled using Canva and BioRender, Created in BioRender. Anita Ioana, V. (2026) https://BioRender.com/mco7g69.

4.1. Alginate: The Reference System and Its Structural Deficits

Alginate is a linear block copolymer of β-D-mannuronate and α-L-guluronate. Its guluronate-rich sequences chelate divalent cations into cooperative junction zones, creating an ionotropic gel within seconds at room temperature and neutral pH [6]. These convenient gelation kinetics underlie its dominance: gelation requires neither radicals, elevated temperature, organic solvent nor photoinitiator, and can be initiated by bath immersion, aerosol, in-nozzle mixing or internal release from a sparingly soluble calcium salt. The resulting

performance depends on grade, formulation, cell population, and crosslinking conditions; representative examples are discussed below. Alginate's limitations are equally established, and they arise from its structure rather than from incidental formulation shortcomings. Native alginate lacks an integrin-binding motif; encapsulated cells therefore remain rounded and mechanotransductively inert unless the polymer is peptide-modified or combined with an adhesive protein. RGD coupling experiments demonstrated this point decisively, restoring adhesion and proliferation only in the modified material [7]. Mammalian cells also secrete no alginate lyase, leaving mass loss dependent on slow, poorly controlled exchange of crosslinking cations for monovalent ions in physiological fluid. Two rational solutions are available. Periodate oxidation introduces hydrolytically labile groups and produces alginate with a tunable degradation rate, albeit with reduced molecular weight and mechanical strength [9]; its dialdehyde product also enables Schiff-base coupling to gelatin, forming the widely used oxidized alginate–gelatin ink family that restores both adhesion and degradability [24]. Alternatively, biorthogonal chemistry offers norbornene–tetrazine click alginate with matrix metalloproteinase-cleavable peptide crosslinks. Here, degradation is executed by the encapsulated cells, converting it from a bulk material attribute into a cell-controlled process [10]. The cited chemistry and three-dimensional culture experiments should not be interpreted as validation of a printed, load-bearing construct. The oxidation route is better quantified. Altering the degree of oxidation of alginate dialdehyde in alginate dialdehyde–gelatin bioinks changes stiffness and network properties monotonically, establishing oxidation degree as the principal single lever trading degradability against mechanical integrity—and making that trade-off a design variable rather than a qualitative caveat [53].

Representative formulations show how these limitations can be addressed selectively rather than simultaneously. In nanocellulose–alginate bioinks, the fibrillar component supplies shear-thinning behavior while alginate provides rapid ionic stabilization [25]. Markstedt et al. demonstrated printing of human chondrocytes, with viability increasing from 73% on day 1 to 86% on day 7 [25]. This example primarily addresses rheology and shape retention; it does not introduce intrinsic integrin-binding motifs into alginate or establish resorption of the cellulose component.

Oxidized alginate–gelatin provides a different division of functions. Oxidation introduces labile sites and aldehyde groups, while gelatin contributes cell-interactive sequences and reactive amines [9,24]. Distler et al. used this formulation to print C2C12 muscle precursor cells and showed that extrusion conditions could guide cell orientation and subsequent myogenic differentiation in vitro [24]. The example therefore connects chemical modification and blending to both processing and biological behavior, while leaving oxidation-dependent mechanical stability as a parameter that requires explicit control.

A third approach combines alginate with silk fibroin methacrylate and sequential stabilization. Kim et al. used ionic pregelation to support deposition and subsequent photocrosslinking to stabilize the printed formulation, reporting improved NIH-3T3 fibroblast compatibility relative to the alginate comparison [54]. This illustrates how immediate shape retention and subsequent network stabilization can be assigned to different components. However, any benefit must be weighed against the additional functionalization and light-exposure requirements rather than attributed to dual crosslinking alone.

Two practical caveats repeatedly matter. First, calcium exposure is itself a cytotoxicity variable, most clearly demonstrated in laser-assisted printing [35]. Second, alginate grades vary sufficiently that formulation parameters cannot be transferred among suppliers or lots without re-characterization [12]; autoclaving also changes molecular weight enough to alter viscoelasticity in a dose-dependent manner, an effect that can be used intentionally but should never pass unmeasured [55]. A further development deserves attention because it

addresses damage rather than mechanics: a dynamic, reversibly bonded alginate bioink with intrinsic antioxidative activity has been reported to attenuate oxidative stress imposed during printing and crosslinking. Cytoprotection, thus becomes a property of ink chemistry rather than medium supplementation alone [56].

4.2. Hyaluronic Acid: Intrinsic Bioactivity Versus Weak Native Mechanics

HA is a non-sulfated glycosaminoglycan comprising alternating D-glucuronate and N-acetyl-D-glucosamine. Native to connective tissue, synovial fluid, skin and brain, it is an active signaling molecule rather than an inert filler [5]. Unmodified high-molecular-weight HA is, however, a viscous and only weakly elastic ink: chains entangle but do not establish a yield-stress network, so filaments spread and layers coalesce. Three dominant approaches address this limitation, each preserving something different.

Supramolecular assembly can supply shear-thinning and self-healing without covalent alteration of the sugar backbone beyond host and guest anchors. Adamantane- and β-cyclodextrin-modified HA forms guest–host networks that shear-flow and recover promptly; they may be printed directly before stabilization by a secondary covalent reaction [57] or extruded into a self-healing support gel of the same chemistry [58]. Covalent photochemistry affords the tightest mechanical control: methacrylated HA cures rapidly under long-wave ultraviolet or visible initiation and is compatible with vat photopolymerization and stereolithography [18,59]. Enzymatic coupling provides intermediate kinetics with high cytocompatibility. In particular, horseradish peroxidase crosslinks tyramine-grafted HA at low hydrogen peroxide and has been implemented in coaxial printing, where enzyme and substrate streams meet at the nozzle [28]. Tandem designs—where a thermoresponsive partner confers temporary shape retention and a photoreaction supplies permanent stabilization—were established early for HA-based cartilage inks and remain a useful template for the wider problem [60]. A fourth strategy partly eases the tension between cure rate and radical dose: ultrafast thiol–norbornene photo-click HA–gelatin inks use step-growth addition rather than radical chain growth, enabling rapid gelation at lower initiator and radical exposure while retaining extrusion compatibility [61]. As discussed in Section 2.4, thiol–ene and acrylate-type photocrosslinkable HA formulations [36]; photochemistry therefore warrants selection and reporting as deliberate as that of the degree of substitution.

Two cautions are especially relevant to HA. Modification degree trades directly against receptor recognition [8], such that aggressively methacrylated HA may function more as a generic polyanionic hydrogel than as HA. HA-based matrices also permit stiffness to be varied independently of ligand density, making them a principal platform for showing that matrix mechanics can dictate phenotype: in patient-derived pancreatic cancer organoids cultured in engineered HA matrices, stiffness itself drove chemoresistance [62]. This sensitivity makes HA valuable for mechanobiology, but uncontrolled variation in crosslink density is an equally serious confounder in tissue-engineering studies.

4.3. Chitosan: Cationic Function Constrained by Solubility

Chitosan, the partially deacetylated derivative of chitin, is the field's principal polycationic polysaccharide. Its protonatable glucosamine amines dissolve the polymer in dilute acid and deprotonate near neutrality, producing pH-dependent solubility, strong polyelectrolyte complexation with polyanions, and the antibacterial and haemostatic behavior that motivates most applications [39]. For bioprinting, this creates a direct incompatibility: the pH that enables processing is not the pH at which cells survive. Three mitigations are established. Thermosensitive formulations containing sodium or magnesium glycerophosphate remain liquid at low temperatures near neutral pH and gel upon warming,

permitting cell-compatible handling [63]. Controlled pH-shift printing instead exploits the neutralization-induced sol–gel transition as the trigger, a route demonstrated for acellular printed chitosan actuators; its compatibility with cells incorporated during printing requires separate validation [64]. Polyelectrolyte complexation with alginate generates composite constructs in which each component offsets the other's weakness; sandwich-structured bioprinted chitosan–alginate dressings with dual drug release exemplify the wound-care application where chitosan's antibacterial activity is most useful [65]. A fourth mitigation relocates the issue to the hardware. In-nozzle homogeneous mixing of alginate, chitosan, and kaolin in a portable bio-pen permits neutralization and complexation at deposition, avoiding prolonged acid exposure for cells and premature gelation in the reservoir [47]. Ink history is another, still insufficiently controlled variable: in chitosan–polyacrylic acid double-network inks, pre-printing ageing time measurably altered printability and post-print performance. Chitosan printability data without a defined ageing protocol are therefore not reproducible, even within one laboratory [66].

For chitosan, acellular scaffolds, printed derivative systems, and native cell-laden formulations should be distinguished because their processing conditions differ [63–66]. Raw-material identity also requires careful specification. Degree of deacetylation, molecular weight and residual protein content differ widely among sources, which is precisely why an ASTM-derived standard-guide framework exists for chitosan raw materials [13].

The examples in Figure 3 illustrate three distinct uses of polysaccharide blending and stabilization rather than interchangeable formulations. The alginate–silk fibroin methacrylate system in panel A combines ionic pregelation with photocrosslinking, as discussed in Section 4.1 [54]. In panel B, the nanoengineered ionic–covalent entanglement (NICE) formulation combines κ-carrageenan, gelatin methacryloyl, and nanosilicates [67]. Chimene et al. demonstrated cell-mediated remodeling and osteogenic matrix formation in printed constructs containing human mesenchymal stromal cells; the anatomical model illustrates fabrication capability, not demonstrated clinical reconstruction of the mandible [67].

Panel C shows the combination of agarose with N,O-carboxymethyl chitosan (NOCC), a chitosan derivative used to formulate cell-containing inks under aqueous processing conditions [68]. Butler et al. varied the blend composition and followed Neuro2A-cell viability in printed constructs over 14 days, identifying a composition-dependent compromise between printability and cellular compatibility [68]. Together, these examples show why a material's contribution must be interpreted within the full formulation. The gelation behavior of agarose and κ-carrageenan is discussed further in Sections 4.6.1 and 4.6.4, respectively.

4.4. Cellulose and Nanocellulose: Rheology Engineering Without Degradability

Because cellulose itself is water-insoluble, bioprinting relies on two derived families. Soluble ethers—methylcellulose and its hydroxypropyl analogue—dissolve in cold water and gel upon heating through hydrophobic association. This thermoreversible behavior is useful for temporary support and can be transformed into permanent structure through dual crosslinking; a dual physically and covalently crosslinked methylcellulose ink illustrates the approach in printing applications [40,69]. Nanocelluloses, by contrast, comprise rigid cellulose nanocrystals and long, entangled cellulose nanofibrils used at low loading as rheology modifiers, where fibrillar entanglement produces pronounced shear-thinning and measurable yield stress. The landmark nanocellulose–alginate bioink established both printability and chondrocyte compatibility [25]. The platform subsequently supported chondrogenic differentiation of induced pluripotent stem cells [70] and human cartilage formation in vivo in bioprinted bacterial nanocellulose constructs [71]. Systematic comparisons of pulp-derived crystals, fibrils and blends showed that morphology—not simply mass fraction—determines printability: fibrils favor yield stress, whereas crystals favor low-

viscosity flow [45]. In soluble form, carboxymethyl cellulose serves a similar rheological role. A tricomposite gelatin–carboxymethyl cellulose–alginate bioink has supported direct and indirect printing of human knee meniscal scaffolds, showing how a cellulose ether can deliver shear-thinning and shape fidelity while contributing little to degradability [72]. Thermoresponsive behavior can likewise be engineered in combination: tuning the sol–gel transition of carboxymethyl cellulose–agarose composite inks enabled complex three-dimensional constructs using physical gelation alone as the printability mechanism [73].

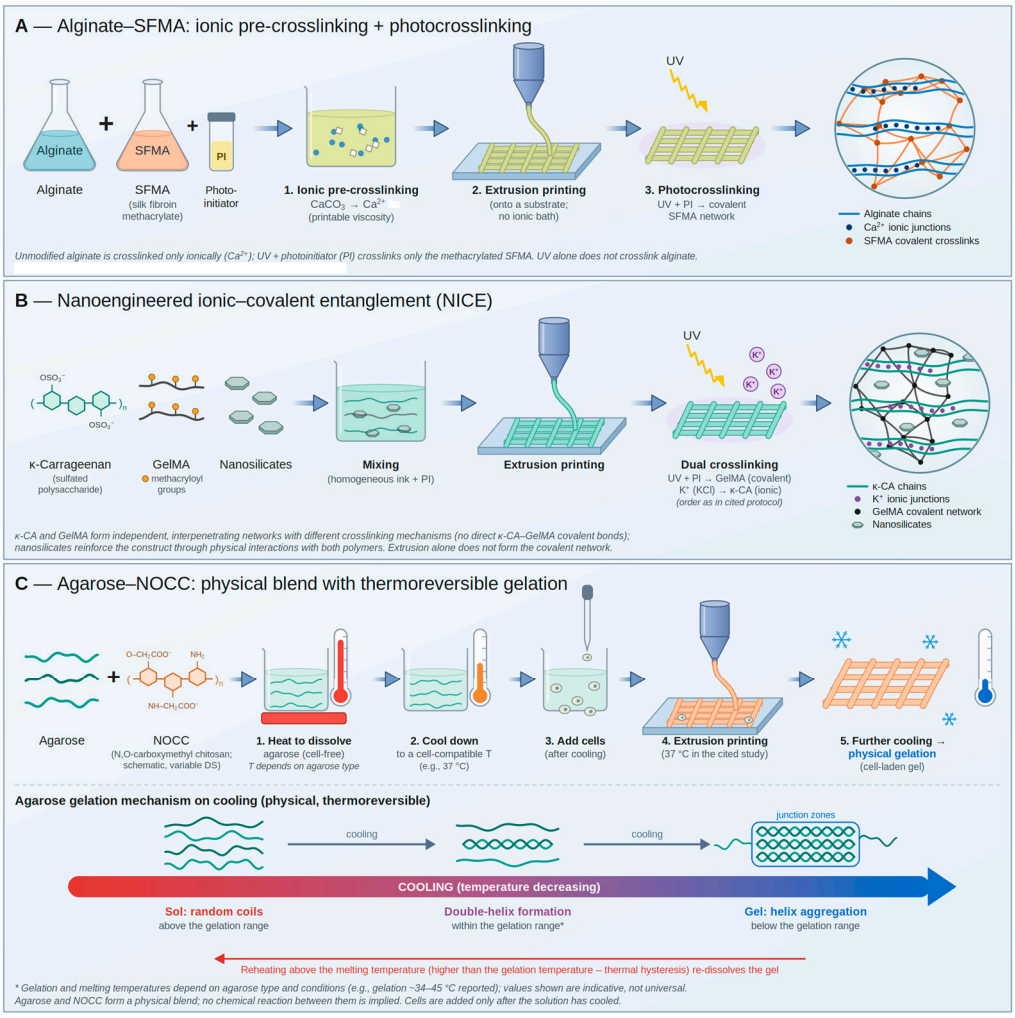

Figure 3. Schematic illustration of multi-component polysaccharide stabilization and network architectures. Conceptual schematic; not to scale. (**A**) Ionic pre-gelation combined with secondary photocrosslinking in an alginate–silk fibroin methacrylate (SFMA) bioink. (**B**) Nanoengineered ionic-covalent entanglement (NICE) integrating κ-carrageenan, gelatin methacryloyl (GelMA), and nanosilicates to achieve dual-network reinforcement. (**C**) Physical blending coupled with thermoreversible gelation for agarose and N,O-carboxymethyl chitosan (NOCC) formulations. Agarose is dissolved by heating in the absence of cells, cooled to a cell-compatible temperature, mixed with cells and extruded; gelation occurs upon further cooling, as disordered chains form double helices that aggregate into junction zones, and the gel re-melts on reheating. Gelation and melting temperatures depend on agarose type and processing conditions, and molecular structures and networks are simplified representations. Created in BioRender. Anita Ioana, V. (2026) https://BioRender.com/yo3tw6v.

To illustrate the diverse stabilization pathways and multi-component network architectures available for polysaccharide bioinks, Figure 3 presents three representative crosslinking strategies. These include ionic pre-gelation paired with subsequent photocrosslinking for alginate–silk fibroin methacrylate systems (Panel A), nanoengineered ionic-covalent entanglement (NICE) combining ionic and covalent crosslinks with nanosilicate reinforcement (Panel B), and physical blending with thermoreversible gelation for agarose–chitosan composite formulations (Panel C). These schematics highlight how structural reinforcement and gelation kinetics can be tailored independently to suit specific biofabrication modalities.

The central limitation is unavoidable: mammalian enzymes do not cleave β-1,4-glucan linkages, and nanocellulose consequently persists within the construct. Two implications follow. It should be treated as a permanent structural additive, paired with a degradable matrix rather than deployed as a sole scaffold; and its long-term host response should be evaluated as for any non-resorbable implant, with fibrous encapsulation and foreign-body reaction as relevant endpoints [11]. Sterilization behavior has been assessed in nanocellulose–alginate–HA bioinks, a necessary precursor to translating this material family [74]. Source matters alongside morphology. Tunicate-derived nanocellulose, an animal-source alternative to plant and bacterial grades, has been assessed in vitro and in vivo for biomaterial performance and biocompatibility, supplying the host-response evidence any non-degradable structural additive needs before translational use [75].

4.5. Gellan Gum: Ordered Networks for Stiff Tissue Targets

Gellan gum is a microbial exopolysaccharide built from tetrasaccharide repeats. It forms transparent, thermoreversible gels through coil-to-helix ordering followed by cation-mediated helix aggregation, and mono- and divalent cations differ substantially in their efficiency [41]. High stiffness at low polymer fraction, optical clarity and glycosaminoglycan-like polyanionic character make it attractive for cartilage-like and optically interrogated constructs. Dedicated reviews of gellan printing inks identify the operative formulation levers—acyl content, ionic strength, temperature programme and blending [76]. Brittleness remains a practical constraint, as do thermal stress at high gelation temperature and rapid, at times poorly controlled, gelation upon exposure to physiological ionic strength. Blending is the usual response: nanofibrillated cellulose–gellan bioinks have enabled skin cell printing [43]; gelatin–gellan systems combine thermoresponsive processing with enzymatic crosslinking for soft-tissue printing [77]; and gellan–dextran methacrylate interpenetrating networks confer covalent permanence and peptide functionalization [44]. Two more recent reports move beyond stiffness alone. A bioprintable gellan gum–lignin hydrogel introduced antioxidant activity and mechanical reinforcement using a bio-derived, rather than synthetic, additive while supporting chondrogenic outcomes, demonstrating that gellan blends can acquire function without synthetic fillers [78]. Gellan has also been recast as a processing medium rather than an ink: granular gellan suspension media with characterized yield stress and self-healing serve as support baths in embedded biofabrication [32].

4.6. Emerging and Complementary Systems

4.6.1. Agarose

Agarose gels on cooling by double-helix formation followed by bundling, yielding a thermally reversible, cell-inert network with well-characterized physical chemistry [40]. That inertness is advantageous for mechanobiology controls but restrictive for tissue formation. Gelatin blending produces extrusion-printable, cytocompatible agarose bioinks for cell encapsulation [79], while molecular tailoring through controlled hydrolysis and derivatization has reconciled printability with the greater stiffness required in stem-cell-mediated bone applications [80]. These outcomes apply to the individual composite formulations rather

than to agarose as a material class. In practice, composite formulation is the route to robust printing: adjusting the thermoresponsive sol–gel window in carboxymethyl cellulose–agarose inks resolved agarose's narrow processing margin while permitting fabrication of complex geometries [73].

4.6.2. Dextran

Dextran is a neutral, highly water-soluble bacterial α-1,6-glucan with a long clinical record as a plasma expander. This provides meaningful regulatory precedent for the raw material, although not for printed constructs. Methacrylation makes dextran a photocrosslinkable network component; gellan–dextran methacrylate interpenetrating networks printed in glycerol and functionalized with RGD derivatives demonstrated both printability and bioadhesion [44], while RGD-grafted dextran methacrylate hydrogels containing osteogenic peptides and manganese oxide nanozymes have been used in bone defect healing [46]. Dextran also appears in tough, self-healing bioinks that permit direct printing of antifatigue cell-laden constructs, a mechanical regime beyond the reach of most polysaccharide gels [81]. Since dextran is bioinert by default, its usefulness depends entirely on grafted functionality—which is also its principal design advantage.

4.6.3. Chondroitin Sulfate

Chondroitin sulfate, a sulfated glycosaminoglycan native to cartilage, is used mainly as a compositional, biomimetic additive rather than as a rheology modifier. Its methacrylated form has entered extracellular matrix (ECM)-biomimetic bioinks that supported in vitro neocartilage formation from bone-marrow mesenchymal stromal cells [82]. Alginate–gelatin–chondroitin sulfate nanocomposites have likewise been reported to induce intrinsic chondrogenic differentiation of human mesenchymal stromal cells without exogenous growth factors; if independently reproduced, this would strongly support compositional biomimicry [83]. Chondroitin sulfate–HA double networks with reversible crosslinks further permit viscoelasticity to be tuned independently of composition [50]. These cell-containing composite and nonprinted hydrogel studies address different questions; their outcomes do not establish a shared level of in vivo performance.

4.6.4. Carrageenan

κ-Carrageenan is a sulfated galactan that forms potassium-ion gels through helix formation, delivering glycosaminoglycan-like sulfation at low cost. Dedicated bioink formulations have defined windows of printability and cytocompatibility [84], and dual ionic-plus-photocrosslinkable κ-carrageenan inks provide the anticipated improvement in post-print stability relative to purely ionic gels [85]. As a minor component, it principally acts as a rheology enhancer, measurably increasing yield stress and shape retention in alginate inks [86]. Host-guest supramolecular gelatin–carrageenan methacryloyl hybrids extend this family to injectable, self-healing wound-healing systems [87]. The principal caveat is biological: sulfated galactans are not inert, and inflammatory responses to particular carrageenan fractions in other settings make explicit reporting of fraction identity and purity essential. Methacrylated κ-carrageenan has also been processed by digital light processing with cell encapsulation, as discussed in Section 2.4 [38].

4.6.5. Pectin

Pectin is a plant-derived galacturonan. Its low-methoxyl fractions gel with calcium through the same egg-box mechanism as alginate, although gelation also depends strongly on pH. This feature has been used deliberately to control kinetics: pH-controlled pectin bioinks built soft three-dimensional neural tissue models, occupying a stiffness regime

inaccessible to stiff polysaccharide gels [42]. Multicomponent pectin–cellulose nanofibre inks improve printability [88], while horseradish peroxidase crosslinking of feruloylated sugar-beet pectin provides a radical-free covalent route [89]. Pectin's main translational barrier is compositional heterogeneity, since degree of esterification, neutral sugar side chains and molecular weight all vary with plant source and extraction route.

Higher plant-derived polysaccharides offer distinct rheological and gelation advantages for extrusion bioprinting. As detailed in Figure 4, different plant-origin polymers can be processed either through dual-network physical-covalent mechanisms (such as hydroxypropyl methylcellulose combined with silk fibroin bioinks for bone marrow-derived mesenchymal stem cell printing, shown in Panel A) or via biofunctionalized covalent crosslinking (such as methacrylated pectin modified with RGD adhesion peptides for human neonatal dermal fibroblast printing, shown in Panel B).

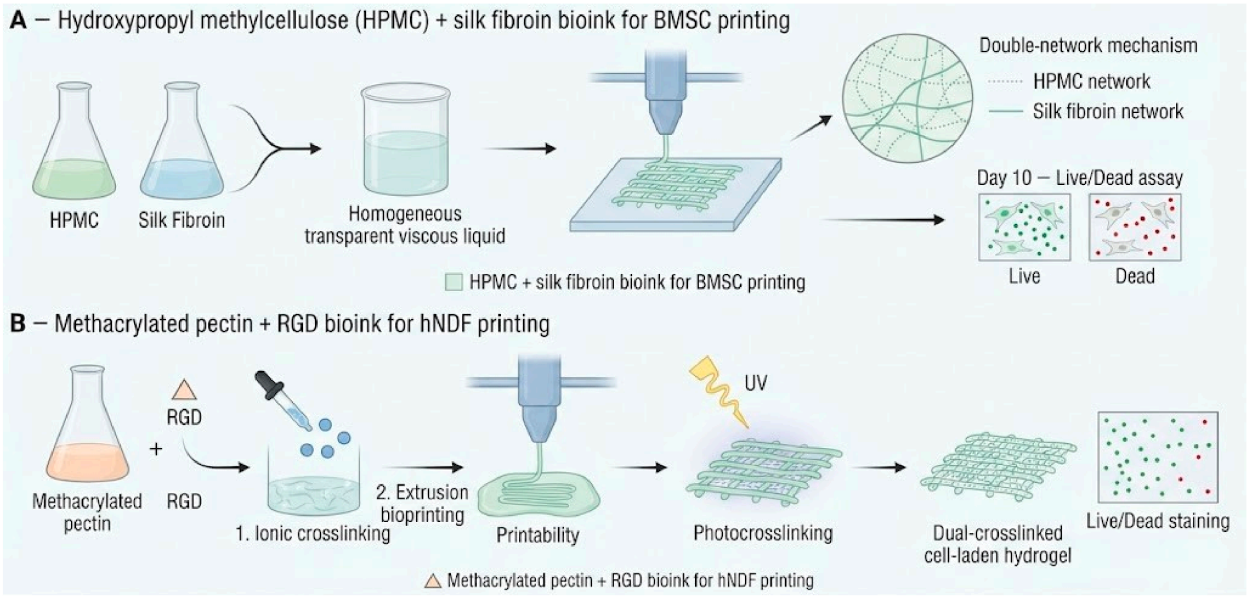

Figure 4. Representative strategies for developing bioprintable formulations from higher plant-derived polysaccharides. Conceptual schematic; not to scale. (**A**) Hydroxypropyl methylcellulose (HPMC) and silk fibroin bioink formulated for the 3D bioprinting and 10-day live/dead viability assay of bone marrow-derived mesenchymal stem cells (BMSCs), featuring a double-network stabilization mechanism. (**B**) Methacrylated pectin functionalized with RGD peptides for extrusion bioprinting of human neonatal dermal fibroblasts (hNDFs), stabilized via sequential ionic crosslinking and UV-induced photocrosslinking. The live/dead panels and the indicated culture time point (day 10) are schematic illustrations created by the authors to show the type of viability assessment applied to such constructs; they do not depict original experimental data. Created in BioRender. Anita Ioana, V. (2026) https://BioRender.com/nae6owb.

4.6.6. Pullulan

Pullulan is a neutral fungal α-glucan with film-forming behavior and reported dermal and wound applications [51,90]. It does not gel spontaneously, so printing requires derivatization or blending.

Norbornene-functionalized pullulan has been combined with a thiol crosslinker to produce photocurable biomaterial inks for digital light processing [37]. Feng et al. demonstrated acellular printing and evaluated hydrogel extracts using L929 cells, rather than assessing cells incorporated during printing [37]. These results support material and fabrication feasibility but do not establish post-printing cell survival, remodeling, or tissue-specific function. Cell-laden polysaccharide-printing claims should therefore not be inferred from this example.

Oxidized pullulan condensed with carboxymethyl chitosan through Schiff-base linkages has also been investigated as an injectable, self-healing, antibacterial hydrogel in an open abdominal wound model [91]. This is an injectable hydrogel precedent rather than direct evidence of a printed cell-laden construct.

4.6.7. Starch

Starch is attractive because of cost, availability and regulatory familiarity, while its amylose–amylopectin composition supplies both linear and branched fractions for network design. Biologically enhanced starch bioinks have supported three-dimensional cell growth [52], and hybrid inks containing methacrylated starch with a minimal fraction of methacrylated chitosan achieved high-precision printing of complex scaffold geometries [92]. Cell-growth and acellular fabrication results should be distinguished from validation of cells incorporated during printing. Retrogradation and amylase-mediated enzymatic digestion also introduce stability variables that bioprinting reports still rarely characterize.

The integrated design logic that connects tissue target, printing modality, structural polysaccharide, and crosslinking chemistry is summarized in Figure 5.

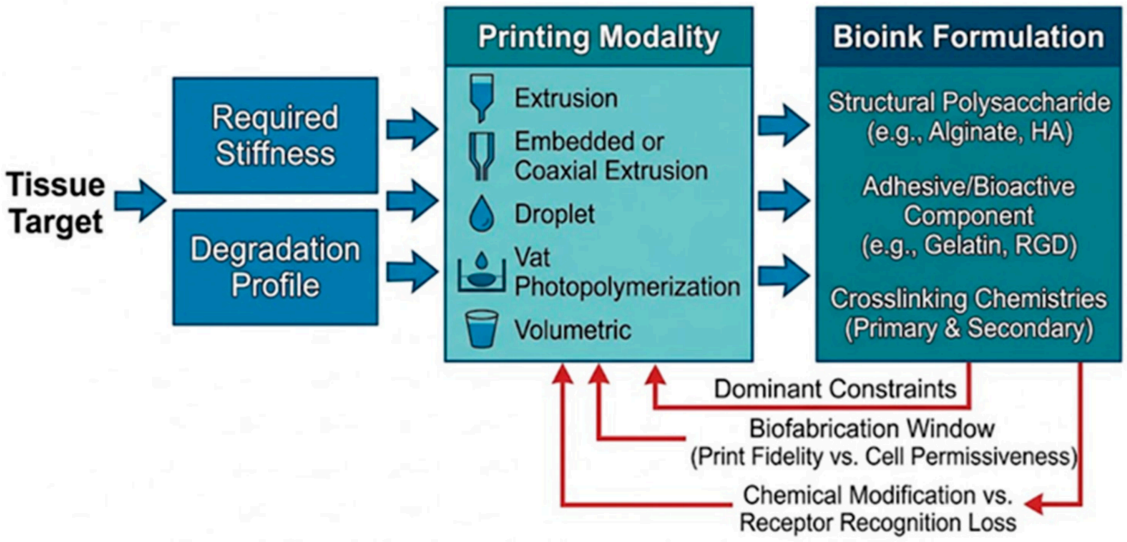

Figure 5. Formulation-design decision map for polysaccharide bioinks. The schematic moves from the tissue target and the required stiffness and degradation profile, through the printing modality (extrusion, embedded or coaxial extrusion, droplet, vat photopolymerization or volumetric), to selection of a structural polysaccharide, an adhesive or bioactive component, and primary and secondary crosslinking chemistries. Feedback arrows denote the two dominant constraints: the biofabrication window between print fidelity and cell permissiveness, and the loss of receptor recognition as chemical modification increases. Original figure created by the authors: individual graphical elements were designed in Canva (Canva Pty Ltd., Sydney, Australia) and assembled into the final figure in BioRender. Created in BioRender. Anita Ioana, V. (2026) https://BioRender.com/jf6bxo1.

To better understand these formulations, Table 1 summarizes the comparative design attributes of core and complementary polysaccharide systems for biofabrication, while study-level examples are provided in Table A1.

Table 1. Comparative design attributes of core and complementary polysaccharide systems for biofabrication. Evidence statements refer to the cited formulation and endpoint, not to every member of the material family or tissue category. The framework and its limitations are defined in Section 1.5; selected study-level examples are provided in Table A1.

Polysaccharide	Charge and Native Gelation	Principal Design Advantage	Principal Limitation	Typical Formulation Strategy	Representative Evidence and Unresolved Validation Needs
Alginate	Anionic; ionotropic with divalent cations [6]	Fast, mild, solvent-free gelation; extensively characterized [6,12]	No integrin ligands; ion-exchange-dependent, poorly controlled loss of integrity [6,7]	RGD coupling; periodate oxidation; gelatin or nanocellulose blends; click crosslinks [9,10,24]	The cited examples address distinct questions: cell-laden nanocellulose–alginate printing [25], functional in vitro oxidized alginate–gelatin constructs [24], and material-specific degradation design [9,10]. These are not interchangeable validation of one formulation.
Hyaluronic acid	Anionic; non-native (viscous solution) [5]	Endogenous glycosaminoglycan with receptor engagement; broad modification chemistry [5]	Weak native mechanics; receptor recognition declines with modification degree [8]	Guest–host supramolecular inks; methacrylation; tyramine–peroxidase coupling; tandem gelation [28,57,59,60]	Acellular light-based fabrication and functional nonprinted hydrogel studies address different questions [36,62]. Evidence must be attributed to the specific formulation and experiment rather than combined into one material-wide level.
Chitosan	Cationic; pH-driven and polyelectrolyte complexation [39]	Antibacterial and haemostatic; complexes with polyanions [39]	Insoluble near neutral pH; source heterogeneity [13,39]	Glycerophosphate thermogelation; pH-shift printing; alginate complexation [63–65]	Acellular fabrication examples and chitosan-derivative cell-containing formulations must be reported separately [63–66]. Native chitosan and soluble derivatives are not assigned a shared maturity level.
Cellulose derivatives and nanocellulose	Neutral to weakly anionic; entanglement, thermal association [40,45]	Strong shear-thinning and yield stress at low loading; high shape fidelity [25,45]	Not degradable by mammalian enzymes; persistence and foreign-body-response risk [11]	Low-loading additive with alginate or gelatin; dual-crosslinked methylcellulose [25,69]	Cell-laden in vitro printing is demonstrated for nanocellulose–alginate [25]. A distinct bacterial nanocellulose formulation has preclinical cartilage-related evidence [71]; neither result establishes class-wide clinical readiness.
Gellan gum	Anionic; thermoreversible helix plus cation bridging [41]	High stiffness at low polymer fraction; optical clarity [41,76]	Brittleness; rapid uncontrolled gelation at physiological ionic strength [76]	Acyl-content tuning; blends with gelatin or nanocellulose; dextran methacrylate networks [43,44,77]	The cited literature includes blended printing formulations [43,44,77] and granular support media [32]. Support-bath performance is not direct evidence of a cell-laden gellan bioink.
Agarose	Neutral; thermoreversible on cooling [40]	Predictable, cell-inert physical network; useful mechanical control [40]	Bioinert; narrow processing window between gelation and cell tolerance [79]	Gelatin blends; molecular tailoring of chain length [79,80]	The cited composite formulations address extrusion compatibility and cell encapsulation [79,80]. Their results are formulation-specific and do not establish application-wide in vivo performance.

Table 1. *Cont.*

Polysaccharide	Charge and Native Gelation	Principal Design Advantage	Principal Limitation	Typical Formulation Strategy	Representative Evidence and Unresolved Validation Needs
Dextran	Neutral; non-native [44]	Blank slate for grafting; clinical precedent as raw material [46]	Requires functionalization for any bioactivity or gelation [44]	Methacrylation; RGD grafting; interpenetrating and self-healing networks [44,46,81]	Functionalized and composite systems address fabrication, adhesion, and tissue-related outcomes in different formulations [44,46,81]. A material-wide evidence level would obscure these differences.
Chondroitin sulfate	Anionic (sulfated); non-native [50]	Compositional biomimicry of cartilage matrix [82]	Minor contribution to printability; limited in vivo evidence [83]	Methacrylated additive in blends; reversible double networks [50,82]	Cell-containing composite printing studies [82,83] should be distinguished from supporting double-network hydrogel studies [50]. No common clinical-readiness grade is assigned.
κ-Carrageenan	Anionic (sulfated); potassium-mediated helix gelation [84]	Sulfated glycosaminoglycan analogue; raises yield stress in blends [86]	Purity and fraction identity affect inflammatory potential [84]	Dual ionic and photocrosslinking; supramolecular hybrids [85,87]	The cited evidence covers distinct extrusion and light-based formulations [38,84,85]. Fabrication, cell compatibility, and tissue-specific function require separate attribution.
Pectin	Anionic; calcium egg-box, strongly pH-dependent [42]	Kinetically programmable gelation; access to very soft matrices [42]	Botanical compositional heterogeneity [88]	pH-programmed gelation; cellulose nanofiber blends; peroxidase crosslinking [42,88,89]	The cited formulations use different blending and gelation strategies [42,88,89]. Their performance must be interpreted with the corresponding cell population and printing conditions.
Pullulan	Neutral; non-native [51]	Film-forming polysaccharide with reported dermal applications [51,90]	No intrinsic gelation; sparse cell-laden data [37]	Photocurable derivatives for light-based printing [37]	Acellular DLP printing and extract-based cytocompatibility are demonstrated for pullulan–norbornene [37]. Cell-laden printing performance is not established by this study.
Starch	Neutral; thermal gelatinization and retrogradation [52]	Low cost, wide availability, familiar raw material [52]	Retrogradation and amylase digestion rarely characterized [92]	Methacrylation; minimal-chitosan hybrid inks [92]	Cell-growth and fabrication results are reported for different modified or hybrid formulations [52,92]. These results do not establish equivalent cell-laden printing performance across starch systems.

5. Crosslinking Strategies: Converting a Printable Fluid into a Stable Network

Crosslinking is the point at which most polysaccharide bioink designs either succeed or fail. It must meet four requirements that are inherently in tension: arrest the printed geometry rapidly, preserve viability under mild conditions, resist dissolution in culture or in vivo for the required period, and remain sufficiently dynamic to allow cell-mediated remodeling. The relative importance of these requirements depends on the application, so crosslinking must be selected together with the printing and culture conditions.

5.1. Ionic and Physical Crosslinking

Ionic bridging remains the most widely used mechanism because it is instantaneous, radical-free, and reversible. Its principal limitation is thermodynamic, not technical: junctions formed by divalent cations are progressively disrupted by monovalent exchange in physiological media, leading to gradual softening and mass loss with kinetics that depend on medium composition and are not easily specified [6]. Ionic crosslinking should therefore be understood as a shape-arresting operation rather than the definitive network. Other physical routes include thermoreversible helix formation in agarose, gellan and κ-carrageenan, hydrophobic association in methylcellulose, hydrogen-bonded entanglement in nanocellulose networks, and polyelectrolyte complexation between chitosan and polyanions. All are cytocompatible and reversible, but all are also sensitive to temperature and ionic strength during handling [40,41,45,65]. Supramolecular host–guest association is distinctive because it combines shear-thinning with self-healing—the rheological combination extrusion most directly demands [57,58].

5.2. Photocrosslinking

Radical photopolymerization of methacryloyl- or norbornene-functionalized polysaccharides affords the greatest control over spatial patterning, crosslink density, and modulus, and remains the only practical route to vat photopolymerization and volumetric printing. Its governing variables—initiator identity and concentration, wavelength, irradiance, exposure time, and oxygen inhibition—are well established, as is the trade-off between cure speed and cytotoxicity driven by radical flux and initiator photolysis products [18,93]. Moving from ultraviolet to visible initiation improves both light-penetration depth and the cellular microenvironment and should be the default when the required modulus remains attainable [94]. Two reporting failures continue to weaken this literature: irradiance and total delivered dose are often omitted, while cytotoxicity is commonly measured only at 24 h, an interval that understates delayed oxidative and genotoxic effects. Where available, thiol–ene chemistries merit preference because their step-growth mechanism lowers radical concentration and produces more homogeneous networks, although the need for thiol-bearing partners remains a real formulation constraint [18]. Within photocrosslinking, chemistry selection is at least as consequential as dose. The comparison of thiolene and acrylate type HA discussed in Section 2.4 illustrates this point inks [36]. Finally, norbornene-based photoclick inks developed specifically for digital light processing likewise form networks at low radical concentration, reinforcing the general preference for step-growth chemistry when a suitable thiol partner is available [95].

5.3. Click and Bioorthogonal Chemistries

Click reactions—strain-promoted azide–alkyne cycloaddition, Diels–Alder cycloaddition, tetrazine–norbornene ligation, and thiol–Michael addition—proceed in water at neutral pH without catalysts or radicals, with kinetics tunable across several orders of

magnitude through substituent choice. Their systematic assessment in extrusion bioprinting identifies the central practical problem: a reaction rapid enough to arrest a filament may also cause the material to gel within the nozzle. Implementation therefore generally depends on in-nozzle mixing, coaxial delivery, or deliberate kinetic retardation [96]. For polysaccharide bioinks, the stronger case for click chemistry is specificity rather than speed. Because the reaction consumes only the introduced handles, cell-instructive peptides can be incorporated as stoichiometric network elements, as demonstrated in protease-sensitive click alginate [10]. Photo-initiated click chemistry offers a useful middle ground by pairing biorthogonal specificity with on-demand triggering: ultrafast thiol–norbornene HA–gelatin inks crosslink within seconds under low-dose irradiation while avoiding the radical chain-growth mechanism responsible for much of the cytotoxicity associated with methacrylate systems [61].

5.4. Enzymatic Crosslinking

Peroxidase-mediated coupling of phenolic substituents is arguably the mildest covalent route available. Tyramine-grafted HA crosslinked with horseradish peroxidase and low hydrogen peroxide has been used in coaxial bioprinting, where enzyme concentration sets gelation rate and thus permits this parameter to be tuned independently of polymer concentration [28]. The same chemistry has been applied to feruloylated sugar-beet pectin, taking advantage of the polymer's native phenolic groups without additional grafting [89]. Transglutaminase and related protein-directed enzymes extend this logic to protein–polysaccharide hybrids, including thermoresponsive, enzymatically crosslinkable gelatin–gellan gum bioinks intended for soft tissues [77]. The limitations are less elegant: cost, control of residual hydrogen peroxide, batch-to-batch variability in enzyme activity, and the need to demonstrate enzyme clearance from the final construct.

5.5. Dynamic Covalent and Dual-Crosslinked Networks

Dynamic covalent bonds—imines and hydrazones formed by aldehyde–amine condensation, boronate esters, and disulfides—yield networks that are covalent but exchangeable, thereby enabling self-healing, injectability, and stress relaxation. Self-healing HA hydrogels based on Schiff-base linkages illustrate both the concept and its dependence on pH and aldehyde content [97]. Combining dynamic crosslinkers with distinct exchange rates provides a direct means of programming stress relaxation independently of stiffness; this is the material property that most clearly separates cell-instructive matrices from those that are merely cell-tolerant [98]. Dual-crosslinked architectures pair a rapid physical or dynamic event with a slower permanent one. Dual-crosslinked methylcellulose [69], ionic-plus-photocrosslinked κ-carrageenan [85], supramolecular-plus-covalent gelatin–carrageenan methacryloyl hybrids [87], and dual-crosslinkable alginate with programmable viscoelasticity that changes mesenchymal stromal cell differentiation outcomes [99] all follow this logic. Recent studies illustrate different functions that dynamic and combined networks can provide [56]. A dynamic, reversibly crosslinked alginate bioink with intrinsic antioxidative activity indicates that dynamic chemistry can mitigate print-induced oxidative stress as well as alter mechanics [56]. Host–guest supramolecular crosslinks added to an alginate network increased toughness and adhesion, quantifying the contribution available from a purely non-covalent secondary network [48]. Anoxidized pullulan-carboxymethyl chitosan injectable hydrogel illustrates the functional potential of dynamic imine networks but does not by itself establish bioprinting performance [91]. Efficient dual crosslinking of a protein-in-polysaccharide bioink has also supported biofabrication of cardiac constructs, among the clearest demonstrations that this design pattern transfers to a demanding tissue target [100]. Dynamic covalent chemistry can further be deployed in flight: coaxial printing

with Schiff-base crosslinking at the nozzle exit generated stable tubular networks that were perfusable immediately after printing, directly coupling network formation to deposition geometry [101].

Dual or sequential crosslinking can separate the rapid stabilization required during deposition from the network properties needed during culture [60,69,85]. However, a second network does not necessarily improve cellular remodeling: depending on its density, lifetime, and connectivity, it may also increase confinement or slow degradation. Its benefit should therefore be tested against a matched single-network or alternative processing strategy, rather than assumed from the presence of two crosslinking mechanisms.

The choice between physical, covalent, dynamic, and combined stabilization depends on the target geometry, culture conditions, and biological endpoint. Table 2 summarizes the principal mechanisms and their limitations; the corresponding measurement and reporting requirements are addressed in Section 6.

Table 2. Crosslinking mechanisms in polysaccharide bioinks: triggers, advantages, limitations, and compatible polymers and modalities.

Mechanism	Trigger	Advantages	Limitations	Compatible Polysaccharides	Best-Suited Modality
Ionic bridging	Divalent or monovalent cations [6]	Instantaneous, radical-free, low cost [6]	Reversible; monovalent exchange causes softening; calcium exposure is itself cytotoxic at high dose [6,35]	Alginate, pectin, gellan gum, κ-carrageenan [41,42,84]	Extrusion, coaxial, droplet
Thermoreversible helix or hydrophobic association	Cooling (agarose, gellan, carrageenan) or heating (methylcellulose) [40]	No chemistry required; useful as transient support [40]	Reversible at body temperature; thermal excursions stress cells [79]	Agarose, gellan gum, κ-carrageenan, methylcellulose [69,76,79]	Extrusion, embedded
Polyelectrolyte complexation	Charge neutralization on contact [65]	Solvent-free; combines complementary polymers [65]	Poor control of network homogeneity; pH-sensitive [39]	Chitosan with alginate, pectin or carrageenan [65]	Extrusion, coaxial
Supramolecular host–guest	Physical association of adamantane and cyclodextrin motifs [57]	Shear-thinning plus self-healing; enables embedded printing [58]	Low modulus alone; requires secondary stabilization [57]	Hyaluronic acid; carrageenan hybrids [57,87]	Extrusion, embedded
Radical photopolymerization	Ultraviolet or visible light with photoinitiator [18]	Rapid, spatially controlled, tunable modulus [18,93]	Radical and initiator cytotoxicity; oxygen inhibition; attenuation with depth [18,94]	Methacrylated hyaluronic acid, alginate, starch, and dextran; norbornene-functionalized pullulan uses radical-mediated thiol–ene chemistry [37,44,59,92]	Vat photopolymerization, volumetric, post-extrusion cure
Click and bioorthogonal ligation	Mixing of complementary handles; catalyst-free [96]	Specific, tunable kinetics, no radicals; peptide crosslinkers possible [10,96]	Nozzle-clogging risk; multi-step synthesis; cost [96]	Alginate, hyaluronic acid, dextran [10,96]	Coaxial or in-nozzle mixing extrusion
Enzymatic phenolic coupling	Horseradish peroxidase with low hydrogen peroxide [28]	Mildest covalent route; rate set by enzyme dose [28]	Enzyme cost and variability; residual peroxide; clearance must be shown [89]	Tyramine-grafted hyaluronic acid, feruloylated pectin, gelatin–gellan [28,77,89]	Coaxial extrusion

Table 2. *Cont.*

Mechanism	Trigger	Advantages	Limitations	Compatible Polysaccharides	Best-Suited Modality
Dynamic covalent (imine, hydrazone, boronate)	Aldehyde–amine or diol–boronate exchange [97]	Self-healing, injectable, programmable stress relaxation [97,98]	pH-dependent stability; creep under sustained load [98]	Oxidized alginate, hyaluronic acid, dextran [24,81,97]	Extrusion, embedded, in situ
Dual and sequential crosslinking	Physical arrest followed by covalent fixation [69]	Can separate deposition-stage shape retention from subsequent network stabilization; benefit is formulation-dependent [85,99]	More process parameters to validate; heterogeneity risk [99]	Most systems; demonstrated for methylcellulose, carrageenan, alginate, hyaluronic acid [60,69,85,99]	All modalities

6. Rheology, Printability and the Standardization Problem

6.1. The Rheological Signature Required by Extrusion

Extrusion requires a rheological profile (Figure 5) matched to the deposition and stabilization route. Shear-thinning can reduce apparent viscosity inside the nozzle and the pressure required for delivery, thereby helping to limit extrusion pressure stays low enough to limit mechanical exposure [16,34]. For unsupported extrusion, sufficient yield behavior or rapid gelation is needed to resist spreading and support overlying layers; yield stress has consequently emerged as one of the more predictive single descriptors of extrusion printability [102]. Recovery of solid-like behavior must occur on a timescale short relative to the deposition interval, a thixotropic-recovery property rather than a steady-state one. Gelation state at the point of extrusion also requires control. Partial pre-gelation improves filament definition but increases shear stress and reduces viability—a coupling quantified in embryonic stem cell bioplotting, where the temperature-controlled gelation state determines both filament quality and viability [23]. These requirements can now be related to the actual flow field rather than inferred from bulk rheometry alone. Combined rheological characterization and computational fluid dynamics modeling predict extrusion behavior and in-nozzle shear history from measured constitutive parameters [103], while dedicated computational analyses quantify how nozzle geometry, applied pressure, and print speed determine wall shear stress and residence time. The consequence is a quantitative basis for treating shear as a dose delivered to cells, rather than as an unmeasured by-product of printing [22]. At a fixed volumetric flow rate and constitutive behavior, reducing nozzle radius increases mechanical exposure. Resolution, flow rate, recovery, and stabilization must therefore be optimized together rather than judged from a single successful lattice. Increasing polymer concentration may improve shape retention while restricting cell movement; whether a secondary network avoids this penalty depends on its density and lifetime, as discussed in Section 5.5 [4,16,69].

Figure 6 separates extrusion into four stages that impose different material requirements. Before extrusion, the formulation must remain sufficiently stable for handling and reproducible delivery. Within the nozzle, its flow behavior and the imposed stress history determine the conditions experienced by the cells; apparent viscosity under flow is therefore more informative than a single viscosity value measured at rest [16,34]. After deposition, structural recovery and any ongoing gelation must limit spreading on the timescale of layer placement. Subsequent stabilization establishes the network that will be exposed to the culture environment, where swelling, ionic exchange, or degradation can alter the initially printed geometry [16,104]. These stages should be characterized separately rather than inferred from a single final image. Geometry and biological function should then be evaluated over a defined follow-up period.

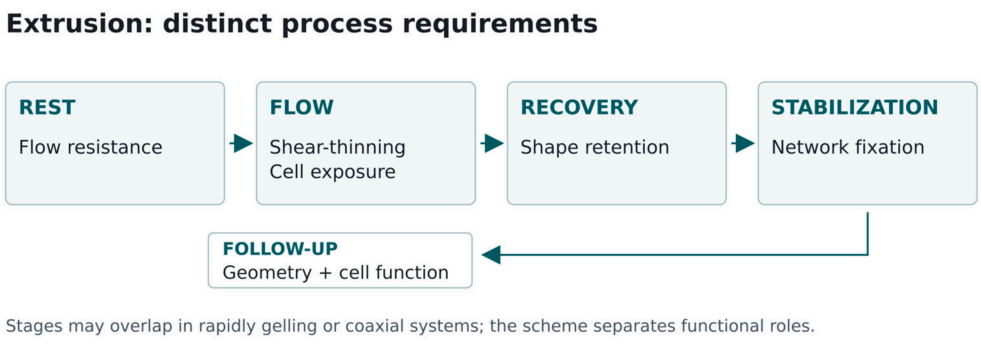

Figure 6. Process requirements during extrusion printing of polysaccharide bioinks. The simplified sequence distinguishes handling at rest, flow through the nozzle, structural recovery after deposition, and subsequent network stabilization. Geometry and cellular function are evaluated after printing and during follow-up. The stages may overlap in rapidly gelling or coaxial systems; the scheme separates their functional roles rather than prescribing a universal temporal sequence. Original schematic.

6.2. From Rheology to Printability Metrics

Rheology alone does not determine print outcome, and the field has appropriately converged on a two-tier assessment. The first tier comprises oscillatory and rotational rheometry: flow curves, amplitude sweeps to identify the yield point, recovery tests, and temperature sweeps where relevant. The second is geometric: filament formation and fusion tests, measurements of strand diameter and uniformity, pore or printability indices derived from lattice prints, and collapse tests on suspended spans [102,104]. Quantitative correlation studies show that particular rheological parameters map to particular print artefacts, allowing defects to be diagnosed rather than simply observed [105]. Dedicated methodological work on precursor rheology of HA hydrogels also illustrates the degree of characterization required if a formulation is to be reproduced elsewhere [106]. Shape fidelity should be measured on the printed construct at the intended cell density, after the intended crosslinking sequence, and following a defined period in culture medium, since swelling and ionic exchange can substantially alter geometry after printing [16,104]. Two developments are especially helpful for the geometric tier. Systematic quantitative analyses of printability indices—filament and pore geometry, spreading, and uniformity—have clarified which indices respond to which formulation change and which offer redundant information [107]. Automated, model-referenced scoring with Hausdorff distance metrics between printed geometry and the digital model replaces subjective visual grading with a continuous, reproducible measurement [108]. On the materials side, systematic variation in oxidation degree in alginate dialdehyde–gelatin inks demonstrates how one chemical parameter can be mapped simultaneously to rheology, stiffness, and print outcome—the form of structure–property evidence that is genuinely useful to other laboratories [53].

6.3. Reporting Practice and Comparability

The practical impediment is not a lack of measurement capability, but a lack of comparability. Laboratories calculate printability indices differently, report nozzle geometries and temperatures inconsistently, and quantify viability using different assays at different timepoints; cross-study comparison of polysaccharide bioinks is consequently often invalid. Two responses are available. The first is disciplined reporting of the minimum parameter set summarized in Table 3, which carries little additional experimental burden. The second is structural: bioprinting should adopt an explicit, rational technology-readiness assessment framework, so claims are graded against defined levels of evidence rather than simply asserted [109]. Such a framework would also make evidence-maturity distinctions explicit at the point of reporting, rather than leaving them to be inferred by readers or

reviewers. Two concrete shortcomings illustrate the scale of the problem. Ink history is rarely controlled: in chitosan–polyacrylic acid double-network inks, pre-printing ageing time alone altered both printability and post-print performance, so a result reported without an ageing protocol is not reproducible [66]. Printability also continues to be claimed from representative photographs rather than calculated, despite the availability of quantitative index frameworks that support cross-formulation comparison [107].

Table 3. Recommended minimum reporting set for rheological and printing characterization of polysaccharide bioinks. Ranges are intentionally omitted because appropriate values depend on formulation and modality; each parameter must instead be measured and reported.

Parameter	Method	Why It Matters	Common Reporting Failure
Flow curve and shear-thinning index	Rotational rheometry over the shear-rate range implied by nozzle and flow rate [16]	Determines extrusion pressure and thus cell shear exposure [34]	Shear-rate range not matched to actual print conditions
Yield stress	Amplitude sweep or stress ramp with a stated determination criterion [102]	Predicts filament collapse and layer stacking [102]	Determination criterion not stated, making values incomparable
Thixotropic recovery	Three-interval or step-shear recovery test with stated recovery percentage and time [16]	Governs shape retention between deposition and crosslinking [16]	Recovery reported qualitatively
Storage and loss moduli, damping factor	Frequency sweep in the linear viscoelastic regime [106]	Distinguishes gel-like from viscous inks before printing [106]	Strain amplitude outside the linear regime
Stress relaxation or creep	Step-strain relaxation with reported relaxation half-time [98,110]	Viscoelasticity, not stiffness alone, governs cell fate [110,111]	Rarely reported at all
Gelation state and temperature at extrusion	Temperature-controlled rheometry plus recorded print-head temperature [23]	Couples filament quality to viability [23]	Print-head temperature omitted
Filament formation and fusion	Suspended-filament and lattice fusion tests [102,104]	Directly measures achievable resolution and pore patency [104]	Single geometry tested; no quantitative index
Shape fidelity over time	Dimensional imaging immediately after print and after defined culture intervals [104]	Captures swelling, syneresis and ionic-exchange-driven change [16]	Measured only immediately after printing
Extrusion pressure, nozzle geometry, speed	Recorded process log [34]	Required to reconstruct shear history and reproduce the print [34]	Nozzle taper and length omitted
Cell density, viability method and timepoints	Characterization of the acellular precursor is reported separately from validation of the cell-laden bioink at the intended printing density [21].	Cells alter rheology; early viability overestimates survival [16,21]	Acellular characterization reported for a cell-laden ink
Crosslinking dose	Cation concentration and exposure time, or wavelength, irradiance and total light dose [18]	Determines modulus, homogeneity and cytotoxicity [18,94]	Irradiance and dose replaced by exposure time alone

Table 3 is intended as a minimum reporting set, not as a universal specification for a successful bioink. Its purpose is to make material, process, and biological outcomes interpretable under stated conditions. Acceptance criteria must be established for the

intended tissue and manufacturing route rather than transferred between formulations solely on the basis of polymer identity.

7. Tissue-Specific Design Requirements and Applications

Tissue targets differ not only in stiffness, but also in the relative priority assigned to mechanical competence, vascular demand, electrical or mechanical function, and permissiveness for migration. Selection of a polysaccharide bioink should follow this weighting, rather than material familiarity (Table 4).

Table 4. Tissue-specific design requirements, representative strategies, and limits of the cited evidence. Evidence statements refer to the cited formulation and endpoint, not to every member of the material family or tissue category. The framework and its limitations are defined in Section 1.5; selected study-level examples are provided in Table A1.

Tissue Target	Dominant Design Requirement	Representative Polysaccharide Strategy	Evidence Scope for the Cited Application	Principal Remaining Limitation
Cartilage and osteochondral	Stiff, glycosaminoglycan-rich, avascular; zonal organization [112]	Nanocellulose–alginate; chondroitin sulfate blends; tandem-gelation hyaluronic acid; gradient printing [25,60,82,113]	Preclinical evidence for a defined bacterial nanocellulose construct containing human chondrocytes [71]; not evidence of restored function in a load-bearing articular defect.	Mechanical properties remain below native articular cartilage; interface and zonal fidelity unresolved [112]
Bone	High modulus with coupled angiogenesis and osteogenesis [114]	Nanostructured multi-material inks; triaxial vascularized constructs; functionalized dextran methacrylate [29,46,114]	Representative multi-material and vascularization strategies are reported [29,114], but fabrication feasibility should not be equated with load-bearing repair. Non-equivalent hydrogel healing studies [46] are identified separately.	Polysaccharide networks alone cannot reach load-bearing modulus; vascular integration immature [29]
Skin and wound repair	Thin, diffusion-supported, antimicrobial, conformal application [115]	Chitosan–alginate dressings; nanofibrillated cellulose–gellan; hyaluronic acid matrices; in situ deposition [43,65,116]	Preclinical in situ printing is illustrated by a porcine burn study [117]. This is not human clinical feasibility, and its formulation should not be assumed to represent the whole polysaccharide class.	Full-thickness skin with appendages and vasculature not achieved [118]
Vascular networks	Perfusable hierarchy down to capillary scale [119]	Carbohydrate and polysaccharide sacrificial templates; photopolymerizable matrices; coaxial sacrificial writing [120–122]	Sacrificial templating and channel-printing studies establish process-specific architectural outcomes [120–122]. Their matrix composition and cellular status must be stated before attributing evidence to a polysaccharide bioink.	Printed channels cannot reach capillary dimensions; requires biological remodeling [119]
Cardiac	Anisotropic, electromechanically coupled, very high cell density [123]	Support-bath and sacrificial roles; blending with decellularized matrix inks [26,124]	Support-medium, collagen, dECM, and hybrid-matrix examples address different roles [26,100,123–125]. Printing an anatomical model is not evidence of functional myocardium.	Polysaccharides provide neither fibrillar architecture nor integrin engagement [125]
Neural	Very low modulus, high permissiveness, guided geometry [126]	Soft hyaluronic acid networks; pH-programmed pectin; channelled guidance scaffolds [42,127]	Pectin bioinks and broader neural-scaffold studies provide different types of support [42,127]. Preclinical outcomes for a cell-loaded scaffold do not establish survival of cells during printing or performance of a different polysaccharide formulation.	Long-term foreign-body reaction and integration with host circuitry [11]
Hepatic	Very high density, oxygen supply, retained metabolic phenotype [128]	Broader organoid-printing and optical-design benchmarks; not all cited matrices are polysaccharide-based [20,129]	The cited volumetric organoid study uses gelatin hydrogels [20] and supports modality design, not polysaccharide-specific evidence maturity.	Oxygen transport and long-term phenotype stability [128]
Tumor and in vitro models	Reproducible, measurable mechanics; no implantation constraint [130]	Polysaccharide tumor models; stiffness-controlled hyaluronic acid matrices [62,130]	In vitro screening evidence must be distinguished from nonprinted HA-matrix mechanobiology [62,130]. In vitro usefulness does not require or imply Level 4 implantation evidence.	Batch reproducibility and standardized mechanical reporting [109]

7.1. Cartilage and Osteochondral Tissue

Cartilage provides a relevant tissue for polyanionic polysaccharide formulations. It is avascular, postponing the vascularization problem; its native matrix is glycosaminoglycan-rich, making polyanionic polysaccharides compositionally plausible; and chondrocytes tolerate a rounded morphology within a confining network. Reviews of cartilage and osteochondral bioprinting document convergence on stiff polyanionic networks supplemented with chondrogenic cues [112]. Nanocellulose–alginate inks supported printing of human

chondrocytes [45] and chondrogenic differentiation of induced pluripotent stem cells [70], while constructs containing human nasal chondrocytes in bacterial nanocellulose were evaluated in nude mice after 30 and 60 days [71]. This is preclinical evidence, not human implantation or load-bearing articular repair. Compositional biomimicry using chondroitin sulfate supplies an additional chondrogenic signal [82,83], and tandem thermal-plus-photo gelation HA inks showed that mechanically adequate constructs can be made without compromising cell compatibility [60]. Zonal organization and the osteochondral interface remain unresolved. Microfluidic print heads that generate continuous cell and material gradients address full-thickness chondral defects directly and currently offer the most promising route to zonal architecture [113]. Even in this relatively favorable setting, printed constructs remain mechanically inferior to native articular cartilage, and long-term functional evidence in load-bearing joints is sparse. Two further primary studies expand the available material strategies. A bioprintable gellan gum–lignin hydrogel combined mechanical reinforcement, antioxidant activity, and chondrogenic support [78]. A tricomposite gelatin–carboxymethyl cellulose–alginate bioink was used for direct and indirect printing of human knee meniscal scaffolds, extending polysaccharide bioinks beyond articular cartilage to fibrocartilage geometries with different mechanical demands [72].

7.2. Bone

Bone presents contradictory requirements: high stiffness and osteoconductivity must coexist with vascular ingrowth, because this metabolically demanding tissue heals through coupled angiogenesis and osteogenesis. Polysaccharides alone cannot provide the required modulus; practical designs are therefore nanocomposites or multi-material constructs. Systematic development of nanostructured multi-material bioinks exemplifies the needed discipline—screening composition against both rheology and osteogenic outcome rather than optimizing either in isolation [114]. Vascular integration has been pursued using triaxial printing that co-deposits an endothelialized channel and an osteogenic matrix in a single step [29]. Dextran methacrylate systems carrying osteogenic peptides and catalytic nanoparticles likewise illustrate how a bioinert backbone can operate as a controlled delivery matrix [46]. Agarose engineered for greater stiffness has been proposed for stem-cell-mediated bone engineering, although the evidence remains early [80]. Viscoelastic programming may matter as much as stiffness: dual-crosslinkable alginate with tunable stress relaxation directs mesenchymal stromal cells toward chondrogenic or osteogenic fates in a relaxation-dependent manner [99,111].

7.3. Skin and Wound Repair

Skin and wound repair are attractive translational targets because constructs can be placed directly on accessible defects and evaluated using defined healing endpoints. However, clinical proximity should not be inferred solely from in situ deposition or the use of human-derived cells. The intraoperative burn study cited here was a preliminary porcine experiment, not treatment of human patients [117]. It supports preclinical feasibility of the reported workflow but does not establish clinical efficacy or class-wide readiness of polysaccharide bioinks. Polysaccharides are well matched to these demands: HA is native to the dermis, chitosan provides antibacterial and haemostatic function, and nanofibrillated cellulose–gellan inks have supported skin-cell printing [43]. Bioprinted human-derived skin organoids accelerated healing of full-thickness defects in vivo, suggesting that biological payload, rather than polymer identity, is the principal determinant of outcome [118]. Two delivery innovations are unusually important in this setting. Handheld, programmable extrusion devices permit conformal in situ deposition over irregular wound beds [113], while the preliminary porcine intraoperative burn study provides a process-feasibility exam-

ple and highlights workflow constraints [116,117]. Chitosan–alginate dressings with dual drug release capture the drug-delivery function that dominates practical wound care [65]. Acellular dressings, cell-laden printed skin, and in situ deposition require separate evaluation; none should be taken as evidence of clinical efficacy for the entire material class. Dynamic covalent polysaccharide systems are particularly well suited to this context. An oxidized pullulan–carboxymethyl chitosan Schiff-base hydrogel that is injectable, self-healing, and antibacterial improved outcomes in an open abdominal wound model, where conformity and infection control are important [91]. This injectable system is not direct evidence of a printed cell-laden construct. On the hardware side, in situ skin bioprinting has been achieved with a commercial articulated collaborative robot—a substantive translational advance because it addresses reach, motion compensation, and clinical-workflow integration rather than ink chemistry alone [131].

7.4. Vascular Networks and the Thickness Barrier

Diffusion restricts viable tissue thickness to a few hundred micrometres from a perfusion source, making embedded vasculature the gatekeeper for every thick-tissue target. Polysaccharides serve three roles. As sacrificial templates, carbohydrate-based materials were used to cast patterned, perfusable networks in the original demonstration of rapid vascular templating [120], and sacrificial-ink strategies followed by endothelialization established multi-material printing of vascularized, heterogeneous constructs [132]. As photopolymerizable matrices, they contribute to multivascular networks with functional intravascular topologies [121]. As support and matrix phases, they enable coaxial sacrificial writing into functional tissue, embedding biomimetic hierarchical vascular networks within dense cellular matrices [122]. Recent synthesis supports a clear strategic conclusion: printed channels alone are inadequate. Printing must be coupled to biological angiogenic remodeling because manufacturable channel diameters do not reach the capillary scale [119]. This remains the field's central open problem and the main reason thick polysaccharide constructs are still preclinical. Embedded printing is pivotal because it decouples ink rheology from shape fidelity and enables sacrificial and coaxial writing of branched, perfusable architectures inside dense matrices [31]. Coaxial deposition with Schiff-base crosslinking at the nozzle exit has formed stable tubular networks that are immediately perfusable after printing, avoiding the delay and dimensional drift associated with post-print bath crosslinking [101]. The broader assessment of microvascularization in engineered tissues and organoids reinforces the same conclusion: printed channels and self-assembled microvasculature operate at different length scales, and hierarchical perfusion will require their combinations rather than either approach alone [133].

Overcoming the diffusion limit in thick engineered tissues requires advanced architectural strategies, such as the incorporation of perfusable fluidic networks. Figure 7 illustrates key structural paradigms for vascularization, ranging from hydrogel microfluidic devices (Panel a) and coaxial extrusion of hollow tubular alginate structures (Panel b) to complex, bioprinted vessel-like networks designed to deliver nutrients throughout larger cellular constructs (Panel c).

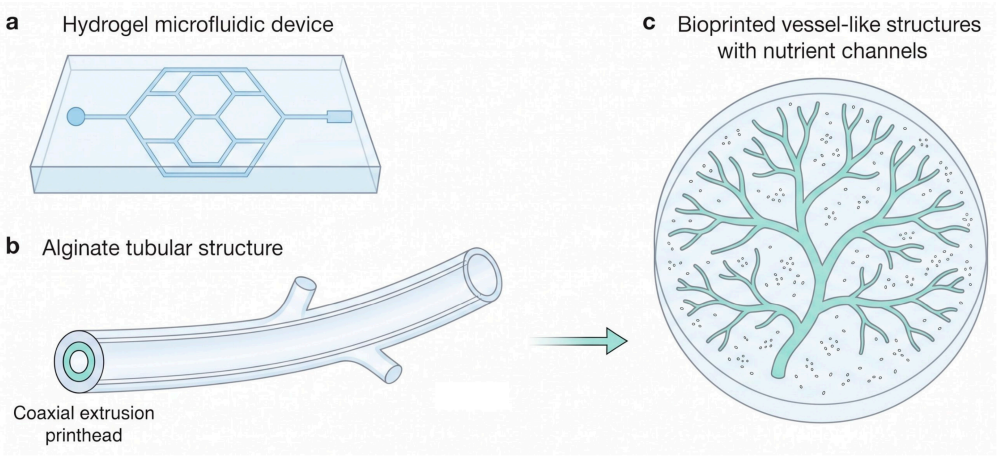

Figure 7. Architectural strategies for vascularization in polysaccharide-based bioprinting. Conceptual schematic; not to scale. (**a**) Design of a hydrogel microfluidic device with internal channel geometries. (**b**) Alginate tubular structure produced via a coaxial extrusion printhead, enabling hollow conduit formation. (**c**) Bioprinted vessel-like branching structures embedded within a nutrient-delivering hydrogel matrix. Dimensions and channel geometries are illustrative only. Created in BioRender. Anita Ioana, V. (2026) https://BioRender.com/73d1wdj.

7.5. Cardiac Tissue

Cardiac applications require anisotropic, electromechanically coupled tissue at high cell density. Polysaccharides are poorly suited as the primary matrix because they provide neither the fibrillar architecture nor the integrin engagement required by cardiomyocytes. Their role is instead as support baths, sacrificial phases, and rheology modifiers: embedded printing in a sacrificial support medium enabled collagen printing of perfusable cardiac components [26,123], and a full-size heart model demonstrated the geometric scalability of this approach [27]. Where matrix biology is decisive, decellularized extracellular matrix bioinks derived from myocardium outperform generic polysaccharide networks and can be tuned for printing [124,125,134]. A more accurate summary is that polysaccharides are enabling process materials, not functional matrices, in cardiac bioprinting. Two recent studies nevertheless indicate a useful contribution. Efficient dual crosslinking of a protein-in-polysaccharide bioink enabled biofabrication of cardiac constructs, with the polysaccharide phase providing printability and the protein phase supplying cell interaction [100]. Nanofibre-assisted embedded extrusion printing has also generated oriented, anisotropic cardiac tissue, confirming that the necessary directional architecture must be imposed by a fibrillar or topographic component that isotropic polysaccharide gels cannot provide [135].

The fabrication of complex anatomical structures—such as cardiac and valvular conduits—demands precise computer-aided design coupled with reliable extrusion deposition and favorable cellular compatibility. Figure 8 outlines this integrated workflow, spanning the initial geometric CAD modeling of a cardiac/valvular conduit (Panel a), the continuous extrusion-based deposition process using a polysaccharide-based hydrogel (Panel b), and the subsequent evaluation of structural integrity and cellular viability following extended static culture (Panel c).

7.6. Neural Tissue

Neural applications invert the usual mechanical requirement: brain and spinal cord are among the body's softest tissues, and stiff networks actively hinder neurite extension. The design requirements are therefore very low modulus, high permissiveness for process outgrowth, and precise geometry to guide axonal alignment [126]. Polysaccharides

contribute in two principal ways. HA is a major component of brain extracellular matrix, making HA-based soft networks compositionally appropriate, while pectin bioinks with pH-programmed gelation have been used specifically to access the very soft regime required for neural models [42]. Geometric guidance has been most convincingly demonstrated with printed scaffolds containing linear channels loaded with neural progenitors, which supported axonal regrowth and functional improvement after spinal cord injury [127]. Foreign-body reaction is a particular concern for chronically implanted neural constructs and interfaces; strategies to control it are therefore directly relevant to non-degradable polysaccharide components [11].

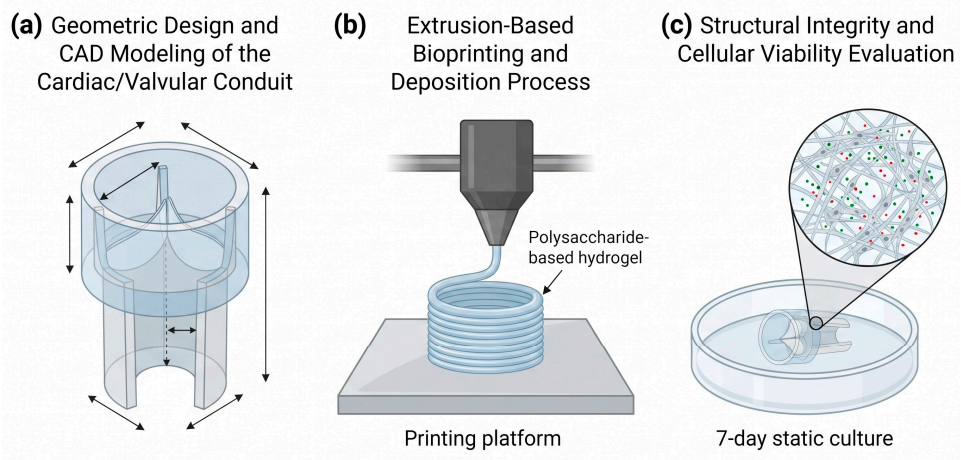

Figure 8. Workflow for the 3D bioprinting of complex anatomical structures using polysaccharide-based bioinks. Conceptual schematic; not to scale. (**a**) Geometric design and computer-aided manufacturing (CAD) modeling of a cardiac/valvular conduit. (**b**) Extrusion-based bioprinting and filament deposition process of a polysaccharide hydrogel on the printing platform. (**c**) Evaluation of structural integrity and cellular viability (via live/dead fluorescence staining) following a 7-day static culture period. The magnified live/dead view and the culture period are schematic illustrations created by the authors and do not depict original experimental data. Created in BioRender. Anita Ioana, V. (2026) https://BioRender.com/k586ove.

7.7. Hepatic Tissue and Metabolic Function

Liver applications require extremely high cell density, oxygen supply, and retention of a drug-metabolizing phenotype; hepatic bioprinting has therefore moved decisively toward organoid payloads. Bioprinted hepatocyte organoids derived from chemically induced pluripotent stem cells have been reported to provide therapeutic function in liver-failure models [128]. Volumetric printing of organoid-laden, gelatin hydrogels demonstrates that optical tuning and construct architecture can support hepatic metabolic endpoints [20]. It is included as a broader process benchmark; the same performance cannot be assumed for a polysaccharide resin. Organoid self-organization provides a complementary biological design principle, but its success in another matrix is not direct validation of a polysaccharide formulation [129]. Embedded sacrificial printing has extended hepatic applications from function to disease modeling: a perfusable hepatic fibrosis model produced by this route reproduced stiffness-driven fibrogenesis. This both demonstrates the capacity for perfused, physiologically graded constructs and reinforces the view that matrix mechanics is an actionable design variable, not an incidental material property [33].

7.8. Tumor Models and In Vitro Testing Platforms

In vitro models are the application in which polysaccharide bioinks are already genuinely useful rather than merely aspirational. Implantation, degradation matching, and

vascular perfusion are unnecessary, while the endpoint is a reproducible biological readout. Polysaccharide hydrogel tumor models have been printed for chemotherapeutic screening [130], and engineered HA matrices showed that stiffness-mediated mechanotransduction drives chemoresistance in patient-derived pancreatic cancer organoids. That finding also cautions against interpreting drug responses from matrices whose mechanics were not measured [62]. Because these platforms inform decision-making rather than implantation, their primary quality requirement is batch-to-batch reproducibility of mechanics and geometry, returning the discussion to standardization [109].

The HA-matrix study is a nonprinted mechanobiology example, included to illustrate how matrix properties can confound a drug-response endpoint rather than to establish printing performance [62].

8. Manufacturing, Sterilization, Quality Control and Regulatory Considerations

8.1. Raw Material Control

Polysaccharides are natural products; their inherent variability is therefore the first serious translational obstacle. Marine and botanical feedstocks change with season and geography, microbial materials with fermentation conditions, and extraction chemistry in turn fixes molecular-weight distribution, residual protein, endotoxin burden and counterion content. This is not a minor analytical nuisance. Two alginate grades assigned the same nominal viscosity can print quite differently, which explains the value of library-scale screening protocols [12]. Standard-guide frameworks for alginate and chitosan used as tissue-engineering raw materials specify the categories a controlled supply must address [13]. Clinical-grade purification of implantable alginate has also shown that endotoxin and mitogenic contaminant control can be achieved, although it demands dedicated processing rather than pharmaceutical-grade sourcing alone [14]. Agency guidance that refers to compendial bacterial endotoxin methods sets the relevant endotoxin-limit and pyrogenicity-testing expectations; these apply directly to polymers of marine and microbial origin [136].

8.2. Sterilization: An Unavoidable Compromise

No sterilization method is neutral with respect to polysaccharides. Moist-heat autoclaving depolymerizes chains by hydrolysis; ionizing radiation generates radicals that cleave glycosidic bonds and may produce either crosslinking or degradation in ways that are not readily predicted; sterile filtration, meanwhile, is constrained by viscosity and cannot accommodate particulate constituents such as nanocellulose. Comparative work on alginate as a bioink component has quantified the extent to which sterilization route changes physicochemical properties and printability and should inform route selection [137]. Serial autoclaving has even been used intentionally to adjust alginate molecular weight and hydrogel viscoelasticity. That usefully converts a degradation mechanism into a process variable, but it also makes plain how substantial the effect can be [55]. For photocrosslinkable precursors, direct comparisons of gamma irradiation and supercritical carbon dioxide treatment show that each modifies subsequent network formation [138]. Sterilization studies of multicomponent nanocellulose–alginate–HA bioinks make a broader point: one route rarely serves every constituent in a blend. Component-wise sterilization followed by aseptic compounding is consequently often the only defensible approach [74]. Sterilization must thus be handled as a formulation variable, with rheological, mechanical and biological characterization conducted on the sterilized material itself. Quantitative studies of terminal irradiation of commercial biomedical hydrogels confirm dose-dependent, measurable shifts in physicochemical and functional properties; post-sterilization re-qualification of rheology and mechanics is therefore not optional [139]. When neither irradiation nor autoclaving is

tolerable, supercritical carbon dioxide treatment is the principal low-temperature alternative. It has achieved effective hydrogel sterilization with limited property loss, although validation remains formulation-specific [140].

8.3. Process Control, Aseptic Manufacture and Critical Quality Attributes

Bioprinting is a manufacturing process with an unusually short and often patient-specific supply chain. Its translational bottlenecks arise predominantly from manufacturing, standardization and characterization, rather than from any shortage of material discoveries [141]. Two documentary frameworks deserve particular attention. In the European Union, good manufacturing practice (GMP) for advanced therapy medicinal products (ATMPs), in force since May 2018 as Part IV of EudraLex Volume 4, defines the expectations for aseptic processing, qualification and risk-based control that clinical bioink manufacture would need to meet [142]. In the United States, agency guidance on additive manufacturing of medical devices describes additive manufacturing as the sequential construction of two-dimensional layers and specifies expectations for device design, process validation and testing. Its remit is devices rather than cell-laden products, a limitation that should be acknowledged explicitly when the guidance is invoked in bioprinting [143]. Biological evaluation of the material itself proceeds through the risk-based approach of the international biocompatibility standard as adopted in agency guidance, with particular relevance to in situ polymerizing systems, absorbable materials and nanomaterials—categories that together encompass most crosslinked polysaccharide constructs, including nanocellulose composites [144]. Table 5 recasts these requirements as a critical-quality-attribute framework for a polysaccharide bioink process. Recent appraisals identify system standardization, interlaboratory reproducibility and the lack of agreed critical quality attributes—not a single unresolved materials problem—as the principal obstacles between laboratory bioprinting and clinical products [15].

Table 5. Indicative critical-quality-attribute (CQA) framework for a clinical-intent polysaccharide bioink process. Since acceptance criteria must be established for each product individually, based on its intended use and performance requirements, no generic values are proposed in this table.

Process Stage	Critical Quality Attribute	Rationale and Control Approach	Primary Reference Basis
Raw polysaccharide	Molecular weight distribution; monomer or substitution composition; counterion content	Governs rheology, gelation and mechanics; control by grade specification and library screening	[12,13]
Raw polysaccharide	Endotoxin, bioburden and residual protein	Marine, botanical and microbial sources carry pyrogen and immunogen risk; compendial endotoxin testing and purification	[14,136]
Functionalized derivative	Degree of substitution and residual reagents	Sets crosslink density and modulus; excessive substitution erodes receptor recognition	[8,18]
Sterilization	Post-sterilization molecular weight, rheology and gelation	Every route alters the polymer; characterization must be repeated on sterilized material	[55,137,138]
Formulation and compounding	Homogeneity, cell density and viability at fill; aseptic assurance	Cells alter rheology; aseptic processing expectations apply to the compounded bioink	[16,142]

Table 5. *Cont.*

Process Stage	Critical Quality Attribute	Rationale and Control Approach	Primary Reference Basis
Printing process	Extrusion pressure, nozzle geometry, speed, temperature, light dose or cation exposure	Defines shear history and crosslink homogeneity; process validation of the build parameters	[18,34,143]
Construct release	Dimensional fidelity; modulus and stress relaxation; sterility; viability and identity	Links the manufactured object to the intended biological performance	[98,104,109]
Biological evaluation	Cytotoxicity, sensitization, degradation products and leachables	Risk-based biological evaluation with specific attention to absorbable and nanomaterial constituents	[144]
In-life and long-term	Degradation kinetics matched to neotissue formation; host response to persistent components	Mismatch causes either mechanical failure or impaired remodeling; persistence raises foreign-body-response risk	[10,11]
Classification and pathway	Cellular content, manipulation level, primary mode of action, matrix role	Determines applicable framework; must be established case by case with the competent authority	[145–150]

Cost and logistics merit rather more attention than they usually receive. Polysaccharide feedstocks are inexpensive relative to recombinant proteins and synthetic peptides, yet medical-grade purification, functionalization chemistry, peptide conjugation and analytical release testing dominate the eventual cost structure. A formulation that relies on several separately synthesized derivatives also multiplies controlled starting materials and their associated documentation burden [13,14]. Formulation parsimony is consequently a genuine translational virtue: a design that meets its purpose with two well-characterized components is preferable to one requiring five components for only marginally better in vitro metrics. Time is equally constraining. Autologous, patient-specific constructs must be manufactured, released and implanted within a window dictated by cell viability rather than convenience, which is the strongest practical case for intraoperative and point-of-care fabrication [116,141].

8.4. Regulatory Classification Is Case-Specific

A bioprinted product cannot be assigned a regulatory class categorically; reviews that attribute one class to every cell-laden construct are misleading. In the United States, the four criteria in the human cells, tissues and cellular and tissue-based products (HCT/P) regulation determine whether a product can be regulated solely under Section 361. One criterion requires manufacture not to combine the cells with another article other than water, crystalloids, or a sterilizing, preserving or storage agent; the others address minimal manipulation, homologous use, absence of systemic effect and independence from the metabolic activity of living cells, except in defined autologous and related situations [145]. A polysaccharide bioink is plainly "another article". A cell-laden polysaccharide construct will therefore generally sit outside Section 361 status and require premarket review, but that result follows from applying the criteria to a defined product, not from a blanket classification. The agency's reading of minimal manipulation and homologous use is set out in dedicated guidance and should be consulted for the particular case [146]. Whether the resulting product is regulated as a biologic, device or combination product depends on its primary mode of action and constituent parts.

In the European Union, advanced therapy medicinal products include gene therapy, somatic cell therapy and tissue-engineered products. A combined advanced therapy medicinal product incorporates one or more medical devices as an integral component; the regulator's own example—cells embedded in a biodegradable matrix or scaffold—maps directly to a cell-laden bioprinted construct [147]. The governing instrument is the advanced therapy regulation of 2007 [148], whereas acellular printed scaffolds and device components of combined products are within the Medical Devices Regulation (MDR) [149]. A classification procedure, legally grounded in the advanced therapy regulation, is available. It is optional, however, and its scientific recommendation is non-binding; it addresses medical-device borderline cases and is issued within 60 days following consultation with the European Commission [150]. The accompanying reflection paper describes the reasoning applied to those borderline products [151]. Comparative analysis of European and United States frameworks for cell-based products shows where definitions, review pathways and evidentiary expectations diverge—an issue of obvious consequence for developers contemplating parallel submissions [152]. A complementary synthesis focused on 3D-bioprinted constructs considers the technological potential of innovative bioinks in relation to these evolving regulatory expectations [153]. The appropriate conclusion for this review is procedural: classification depends on cellular content, degree of manipulation, intended use, primary mode of action and the role of the matrix, and must be determined case by case with the relevant authority.

8.5. Long-Term Safety

Two long-term questions remain systematically under-reported. The first concerns degradation-product fate: oxidized alginate releases low-molecular-weight fragments, photocrosslinked networks retain unreacted methacrylate groups and initiator photolysis products, and dynamic covalent networks liberate small aldehydes during hydrolysis. Each falls within the biological-evaluation expectations for leachables and degradation products [9,144]. The second concerns reactions to non-degradable constituents. Nanocellulose persists indefinitely, and persistent implants provoke foreign-body responses whose control is an active field in its own right; the relevant assessment horizon is the intended life of the implant, not the duration of a conventional study [11,141]. For nanocellulose, specifically, source-resolved biocompatibility evidence is now available. Tunicate-derived nanocellulose has been evaluated in vitro and in vivo, the kind of evidence required before a non-degradable structural additive is advanced into a clinical-intent formulation [75].

8.6. Translational Barriers and Published Solutions: A Synthesis

The translational barriers facing polysaccharide bioinks are neither peculiar to this material class nor wholly generic. Each has appeared repeatedly in the primary literature, and each has at least a partial published remedy. Table 6 sets them out systematically, linking the principal barriers identified across Sections 4–8 to their root causes and to the published solutions supported by citations. It should be read as a practical checklist for teams planning translational work: the more barriers a formulation has already addressed, with evidence appropriate to the intended application, the shorter its remaining translational path.

Table 6. Principal translational barriers, their causes, and published mitigation approaches. The final column distinguishes experimental support, methodological synthesis, and regulatory or standards documentation. The existence of a published mitigation strategy does not demonstrate that the corresponding barrier has been resolved for a clinical product.

Barrier	Root Cause	Published Mitigation Approach	Reference Basis and Scope of Support
Raw-material variability and inter-batch drift	Marine, botanical and microbial polysaccharides vary with source, season and fermentation conditions; molecular weight (MW), substitution pattern and residual protein shift between batches	Adopt medical-grade specification frameworks with defined ranges for MW, substitution, endotoxin and residual protein; library-scale screening before formulation lock	Experimental characterization and standards-related guidance [12–14]; raw-material control, not clinical performance.
Sterilization-induced degradation of bioink components	Autoclave hydrolysis, gamma-radiation radical cleavage and filtration exclusion of nanocomponents each alter rheology and mechanics unpredictably	Sterilization treated as a formulation variable; component-wise sterilization plus aseptic compounding; supercritical CO_2 as low-temperature alternative for sensitive precursors; re-characterization after sterilization mandated in the CQA framework	Experimental sterilization studies and methodological guidance [74,137–140]; applicability must be tested for each formulation.
Cell shear damage during extrusion	Cell response depends on stress magnitude, exposure duration, cell type, nozzle geometry, and gelation state.	Match nozzle geometry, flow rate, and rheology; validate viability and later function at the intended cell density.	Primary mechanical-exposure studies, computational modeling, and methodological synthesis [21–23,34]; method-specific support.
Loss of receptor recognition on chemical modification	HA modification can alter receptor engagement; the effect depends on substitution chemistry, degree, and presentation [8].	Quantify receptor-related activity alongside substitution and network mechanics; compare against appropriately matched controls.	Primary nonprinted matrix studies [8,110,111]; mechanistic support, not direct evidence of printed-construct performance.
Nozzle clogging and shear inactivation of click reactions	Fast bio-orthogonal chemistries partially advance in the nozzle before extrusion, changing viscosity and blocking flow	Two-component coaxial extrusion; delayed activation by pH, temperature or light; slower click chemistries paired with a fast physical primary network	Primary formulation study and chemistry review [10,96]; reaction-specific design guidance.
Poor filament recovery and shape fidelity	Insufficient yield stress or slow gelation kinetics cause filament spreading and layer collapse	Dual physical–covalent crosslinking; increased yield stress via nanocellulose or self-healing supramolecular blends; reporting recovery time and layer-stacking limits explicitly	Quantitative printability and rheological studies [16,102,104]; process-specific rather than clinical validation.

Table 6. *Cont.*

Barrier	Root Cause	Published Mitigation Approach	Reference Basis and Scope of Support
Incomparable printability metrics across laboratories	Printability indices, filament collapse tests and yield-stress determinations use non-standardized methods, geometries and criteria	Adopt shared minimum reporting set (Table 3); explicit statement of yield-stress determination criterion; report shear-rate range matched to actual print conditions	Methodological synthesis and quantitative printability studies [16,102,104,107–109]; reporting support.
Regulatory classification ambiguity for cell-laden constructs	Classification depends on cellular content, degree of manipulation, mode of action and matrix role, and is case-specific in both US and EU frameworks	Treat classification as a design question during formulation; use the EU optional classification procedure; align with EU ATMP GMP or FDA guidance on additive manufacturing as appropriate to product type	Regulatory and agency documents and comparative regulatory analysis [145–152]; procedural basis only, not evidence of clinical performance.
Foreign-body response to persistent structural additives	Non-degradable components (nanocellulose, some methacrylated networks) persist beyond the intended implant life and can drive chronic inflammation	Match persistence to intended use; combine non-degradable structural additive with degradable matrix; report degradation over implant-relevant timescales	Experimental host-response evidence and safety-related syntheses [11,75,144]; material- and use-specific.
Vascular thickness barrier in bulk constructs	Diffusion distances limit oxygen and nutrient supply in bulk constructs; the limiting thickness depends on demand, geometry, and transport conditions.	Sacrificial coaxial and embedded printing of endothelial-lined channels; hierarchical branching with pre-vascular polysaccharide inks; co-printing of endothelial cells and angiogenic factors	Vascular and broader biofabrication syntheses [119,122,133]; architectural rationale, not a universal viable-thickness limit.
Cardiac anisotropy and electromechanical coupling deficit	Isotropic polysaccharide gels do not support the directional myofiber alignment or electrical propagation required for functional myocardium	Fiber-assisted embedded extrusion for directional architecture; conductive fillers; anisotropic printed geometries with cardiac-specific ECM components	Material/process examples and methodological syntheses [100,125,135]; not regulatory or clinical-efficacy evidence.

Two broader observations arise from Table 6. First, several obstacles reside at the formulation rather than material level. Raw-material variability, sterilization compatibility, non-comparable printability metrics and regulatory classification reflect choices concerning supplier specifications, sterilization route, reporting practice and product-mode-of-action determination within a material family; their solutions are correspondingly procedural and documentation-based, not demands for new chemistry [12–15,137,145–147]. Second, the most resistant problems—the vascular thickness barrier and the electromechanical anisotropy deficit of polysaccharide-based cardiac constructs—require added design elements, including fibrillar reinforcement, hierarchical channel architectures and conductive fillers, that isotropic polysaccharide gels cannot furnish alone [100,125,135]. Recogniz-

ing the difference matters. It prevents the recurrent mistake of offering a chemistry-only response to an essentially architectural problem.

9. Future Directions

9.1. Dynamic and Granular Architectures for Processability and Cellular Remodeling

Future formulations should consider how mechanics evolve over time and across structural scales, rather than using initial stiffness as the sole design target. Molecularly dynamic networks and granular assemblies approach this problem at different levels: the former regulate network rearrangement through reversible interactions, whereas the latter introduce particle rearrangement and interparticle voids. Their common objective is to provide processability without imposing unnecessary long-term constraints on cells.

At the molecular scale, alginate-based hydrogel studies have shown that stress-relaxation rate can be varied independently of initial elastic modulus and can alter cell spreading, proliferation, and osteogenic differentiation [110]. These nonprinted mechanobiology experiments establish a design rationale rather than direct evidence of printing performance. Dynamic crosslinkers with different exchange kinetics offer routes to tune relaxation, while dual-crosslinkable alginate systems illustrate how viscoelastic design can be linked to differentiation outcomes [98,99]. Translation of these findings into bioinks requires confirmation that the relevant relaxation behavior persists after the complete printing and stabilization process.

At the particle scale, granular bioinks are assembled from microgels whose packing and interparticle interactions can provide yield behavior and flow under shear [154]. Their connected void space can offer routes for transport and cellular movement that differ from the molecular mesh of a homogeneous hydrogel. These advantages are not guaranteed: particle size and deformability, packing fraction, and post-print annealing determine whether the construct remains sufficiently porous, cohesive, and dimensionally stable [154]. Granular formulations should therefore be compared with bulk gels using matched composition and clearly defined mechanical and biological endpoints.

Polysaccharides can contribute either as the microgel building blocks or as granular support media. Gellan gum suspension media, for example, have been investigated as support baths for embedded biofabrication [32]; this role must be distinguished from that of a cell-containing granular bioink. The most useful next step is not to favor one architecture categorically, but to identify which combination of reversible interactions, particle organization, and stabilization meets a defined tissue requirement. The relevant reporting parameters are consolidated in Table 3, with particle-size distribution, packing, and interparticle bonding added when a granular architecture is used.

9.2. Extracellular Matrix Mimicry and Hybrid Composition

Decellularized extracellular matrix (dECM) bioinks offer tissue-specific biochemical complexity that no defined polysaccharide can recreate, but their printability is poor and their composition variable. Polysaccharides, in contrast, afford printability and defined mechanics while supplying limited biochemical information [125,134]. Hybridization is therefore both chemically and biologically well-reasoned; the substantive design question is which component should govern each property. A related strategy is minimal biomimicry: instead of adding whole matrix, introduce the particular glycosaminoglycan or peptide sequence shown to be necessary, as with chondroitin sulfate supplementation for chondrogenesis [83] or protease-cleavable peptide crosslinks that enable cell-controlled degradation [10].

9.3. Vascularization and In Situ Fabrication

Finer nozzles will not solve vascularization. A more productive strategy couples printed mesoscale channels to biological angiogenic remodeling and uses support-bath and sacrificial polysaccharide chemistries to embed hierarchical networks within dense cellular matrices [119,122]. In parallel, in situ intraoperative bioprinting avoids several manufacturing and logistics constraints by fabricating directly within the defect, albeit under stringent limitations of sterility, speed, crosslinking chemistry and quality control [115–117]. Both approaches favor polysaccharides because their gelation is mild and rapid. Hardware maturity is also advancing: in situ skin bioprinting has been demonstrated with a commercial articulated collaborative robot [131]. Yet the microvascularization literature makes clear that the biological part of the problem—endothelial self-assembly into capillary-scale networks in the printed matrix—will determine whether such constructs perfuse at clinically useful thickness [133].

9.4. Computational Formulation Design

Bioink development remains substantially empirical. The combinatorial space spanning polymer identity, concentration, molecular weight, modification degree, crosslinker chemistry and process parameters is simply too large for exhaustive screening. Machine-learning models trained on formulation and process descriptors have predicted and optimized printability [155], while constraint-based Bayesian optimization of bioink precursor design has reduced the experiments required to reach a target [156]. The limiting factor is data quality: a model can transfer only as well as the reporting standards of the literature on which it is trained, returning the argument to Section 6.3 [16,109]. Two complementary advances make the problem more manageable. Automated, model-referenced printability scoring using Hausdorff distance metrics supplies the consistent continuous labels that data-driven models need [108]. Coupling measured rheology with computational fluid dynamics also replaces purely empirical descriptors with physically grounded features—predicted wall shear stress, residence time and extrusion profile [103].

9.5. Higher-Order Biological Payloads

The payload is now becoming as consequential as the matrix. Printing organoid-forming stem cells, rather than dissociated cells, allows the print pattern to template macroscale tissue self-organization while the biology resolves the fine architecture [129]. Organoid-laden constructs have already generated measurable hepatic and therapeutic functions [20,128]. For polysaccharide bioink design, this shifts the relevant requirements toward mesh sizes and relaxation timescales that allow organoid growth and fusion, and toward modalities that which impose no nozzle shear, such as volumetric and dynamic interface printing [19,157].

9.6. Research Priorities for the Next Cycle

Taken together, Sections 2–9 point to seven priorities for the next translational cycle of polysaccharide bioinks. They are ordered, approximately, along the design chain developed in this review.

(i) Treat viscoelastic and dynamic mechanics as primary, not secondary, design targets, using dual-crosslinked or dynamic covalent architectures with a stress-relaxation timescale engineered for the target tissue [110,111,158].

(ii) Advance granular and microgel bioinks beyond laboratory demonstrations toward standardized formulations that report bead-size distributions, packing fractions and interparticle chemistries, thereby making comparative studies possible [154].

(iii) Couple angiogenesis with osteogenesis, and angiogenesis with cardiogenesis, from the outset through hierarchical channel architectures, sacrificial polysaccharide inks and biological cues co-printed with the structural component [159,160].

(iv) Develop and share computational formulation-design pipelines—coupled rheology–printability–viability models, Bayesian optimization of precursor space and machine-learning-assisted screening—to reduce the empirical burden of multicomponent formulation design [155,156].

(v) Implement a shared minimum reporting standard for bioink rheology, printability and cell-laden functional endpoints (Table 3), such that inter-laboratory reproducibility becomes tractable [15,16,109].

(vi) Characterize sterilized material at the intended cell density and print modality, and require this practice in submissions to translationally oriented journals; the sterilization–printability–viability chain remains the field's most consistently under-reported characterization gap [74,137–140].

(vii) Treat regulatory classification as a design question, rather than a compliance appendix, so that a bioprinted construct's primary mode of action, matrix role and cellular content are considered during formulation rather than afterward [145–153]. None of these priorities is individually new—most have already been proposed in the primary literature. Their joint adoption within one formulation programme, and reporting of them as a package, would nevertheless materially shorten the distance between the present preclinical state of polysaccharide bioinks and clinical products.

9.7. Limitations of the Present Review

This review has several limitations. Literature selection was narrative and expert-curated rather than based on a prospectively registered systematic-review protocol. The tables therefore provide representative, traceable examples rather than an exhaustive study inventory, and publication bias towards favorable printing or biological outcomes cannot be quantified.

The five-level framework describes the experimental setting and validation endpoint of an individual study; it is not a validated certainty assessment or a numerical measure of clinical readiness. Independent replication, study design, follow-up, and relevance to the intended tissue remain separate considerations. Mechanistic findings from nonprinted hydrogels, acellular fabrication results, and advances demonstrated in non-polysaccharide matrices are explicitly distinguished from direct cell-laden polysaccharide-printing evidence.

Finally, differences in formulation, cell type, printing equipment, crosslinking exposure, and outcome measurement prevent robust pooling of reported moduli, printability indices, and viability values [16,109]. Numerical examples are therefore attributed to individual experimental conditions rather than used as universal operating windows or comparative rankings. The conclusions identify design priorities supported by the cited literature, not the proportion of all published formulations that has reached a given developmental stage.

10. Conclusions

Polysaccharides provide chemically diverse platforms for biofabrication, but their suitability depends on the function assigned to each component within a defined process. Native gelation, charge, substitution, molecular weight, and degradation behavior influence both fabrication and cell–matrix interactions. These relationships support rational

formulation design, provided that improved shape fidelity is not taken as evidence of tissue function or clinical readiness.

The central need is for studies that link composition and processing to sustained, application-relevant biological outcomes. Dynamic or sequentially stabilized networks, granular architectures, and support-bath approaches can help separate processing requirements from the cellular microenvironment, but no strategy is optimal for every tissue. Reproducible reporting, validation after sterilization, characterization at the intended cell density, and product-specific quality and safety assessment are essential to determine whether a promising formulation can progress beyond a laboratory demonstration. The next translational gains should therefore come from integrated validation of defined formulations and manufacturing processes rather than from increasingly complex material combinations alone.

Author Contributions: Conceptualization, A.I.V., R.C., A.B., A.P. and N.D.B.; methodology, A.I.V. and A.B.; validation, A.I.V., A.B., A.P. and N.D.B.; formal analysis, A.I.V. and A.B.; investigation, A.I.V., A.B., A.P. and N.D.B.; resources, A.I.V., A.B. and A.P.; data curation, A.I.V. and A.B.; writing—original draft preparation, A.I.V., R.C. and A.B.; writing—review and editing, A.I.V., R.C., A.B., A.P. and N.D.B.; visualization, A.I.V., R.C. and A.B.; supervision, A.I.V., R.C. and A.P.; project administration, A.I.V.; funding acquisition, A.I.V. All authors have read and agreed to the published version of the manuscript.

Funding: This research was funded by the Romanian Ministry of Research, Innovation and Digitalization under the Romanian National Nucleu Program LAPLAS VII—contract No. 30N/2023 and by Project SMIS code 341960, "Artificial Intelligence-Based Solution for the Monitoring, Digitalization, Computerization and Optimization of Intraoperative Processes in High-Risk Surgery, with the Aim of Reducing Nosocomial Infections," co-financed by the European Regional Development Fund (ERDF) under the Health Programme 2021–2027, Priority P9—Contribution to the STEP Platform: Biotechnology and Digital Technologies, including Associated Services in the Health Sector. R.C. acknowledges the financial support received from the Research Institute of the University of Bucharest (ICUB) under the research fellowship programme "Fellowships for Visiting Professors", Contract no. 6434/08.07.2026.

Institutional Review Board Statement: Not applicable. This review does not report studies involving humans or animals.

Informed Consent Statement: Not applicable. This review does not report studies involving human participants.

Data Availability Statement: No new data were created or analysed in this study. All information discussed is available in the cited publications and in the cited regulatory and standards documents.

Acknowledgments: During the preparation of this manuscript, the authors used ChatGPT-3.5 for English language polishing, grammatical corrections, and synonym selection. The authors subsequently reviewed and edited the content as necessary and took full responsibility for the integrity, accuracy, and originality of the final manuscript. The graphical abstract was created with BioRender.com. Publication license: https://BioRender.com/cxfyno8. Some elements were designed in Canva (Canva Pty Ltd., Sydney, Australia, https://www.canva.cn/en/, accessed on 10 August 2026).

Conflicts of Interest: The authors declare no conflicts of interest. The Canva Pty Ltd. had no role in the design of the study; in the collection, analyses, or interpretation of data; in the writing of the manuscript, and in the decision to publish the results.

Abbreviations

3D	three-dimensional
ATMP	advanced therapy medicinal product
CQA	critical quality attribute
dECM	decellularized extracellular matrix
ECM	extracellular matrix
GMP	good manufacturing practice
HA	hyaluronic acid
HCT/P	human cells, tissues, and cellular and tissue-based product
MDR	Medical Devices Regulation (Regulation (EU) 2017/745)
RGD	arginine-glycine-aspartate adhesion motif
ADA	alginate dialdehyde
DLP	digital light processing
GelMA	gelatin methacryloyl
NICE	nanoengineered ionic–covalent entanglement
NOCC	N,O-carboxymethyl chitosan
nSi	Nanosilicates
SFMA	silk fibroin methacrylate

Appendix A. Illustrative Study-Level Evidence Attribution

Table A1. Illustrative study-level application of the evidence framework. This traceable subset is not an exhaustive extraction of all studies cited in the review.

Study and Experimental Context	Directly Supported Evidence	Classification and Boundary
Markstedt et al. [25], nanocellulose–alginate with human chondrocytes	Cell-laden printing; viability of 73% and 86% after 1 and 7 days, respectively.	Level 2 for the viability claim. These values do not establish mature cartilage function.
Distler et al. [24], printed oxidized alginate–gelatin with C2C12 cells	Cell orientation and myogenic differentiation in vitro following extrusion.	Level 3 for this formulation and endpoint; not in vivo muscle regeneration.
Apelgren et al. [71], printed bacterial nanocellulose constructs with human nasal chondrocytes	Implantation in nude mice with evaluations after 30 and 60 days.	Level 4. Human cell origin does not make this a human clinical study; the result is not evidence of load-bearing joint repair.
Feng et al. [37], photocurable pullulan–norbornene	Acellular DLP printing and separate L929-cell testing using hydrogel extracts.	Level 1 for printing feasibility; no claim of survival of cells during printing.
Steudter et al. [36], photocrosslinkable HA inks	Comparative photochemistry and DLP fabrication; 4% w/v HA formulations produced 100 µm holes within 2 s under the reported conditions.	Level 1 for the fabrication claim; these data do not themselves establish cell-laden biological performance.
LeSavage et al. [62], HA-containing engineered matrices with patient-derived pancreatic organoids	Nonprinted in vitro mechanobiology and chemoresistance.	Supporting mechanistic evidence, outside the printing levels. Patient-derived cells are not clinical implantation evidence.
Albouy et al. [117], intraoperative deposition in a severe-burn model	Fibroblast-containing material printed onto experimentally induced wounds in a pig.	Preclinical Level 4 for the reported process; not human feasibility. This is used as a process example; no polysaccharide-specific attribution is made here.
Bernal et al. [20], organoid-laden gelatin hydrogels	Volumetric printing and liver-related metabolic functions.	Supporting non-polysaccharide modality evidence, not a level assigned to a polysaccharide formulation.

References

1. Murphy, S.V.; Atala, A. 3D bioprinting of tissues and organs. *Nat. Biotechnol.* **2014**, *32*, 773–785. [CrossRef] [PubMed]
2. Groll, J.; Burdick, J.A.; Cho, D.W.; Derby, B.; Gelinsky, M.; Heilshorn, S.C.; Jüngst, T.; Malda, J.; Mironov, V.A.; Nakayama, K.; et al. A definition of bioinks and their distinction from biomaterial inks. *Biofabrication* **2019**, *11*, 013001. [CrossRef] [PubMed]
3. Levato, R.; Jungst, T.; Scheuring, R.G.; Blunk, T.; Groll, J.; Malda, J. From Shape to Function: The Next Step in Bioprinting. *Adv. Mater.* **2020**, *32*, 1906423. [CrossRef] [PubMed]
4. Malda, J.; Visser, J.; Melchels, F.P.; Jüngst, T.; Hennink, W.E.; Dhert, W.J.A.; Groll, J.; Hutmacher, D.W. 25th Anniversary Article: Engineering Hydrogels for Biofabrication. *Adv. Mater.* **2013**, *25*, 5011–5028. [CrossRef] [PubMed]
5. Burdick, J.A.; Prestwich, G.D. Hyaluronic acid hydrogels for biomedical applications. *Adv. Mater.* **2011**, *23*, H41–H56. [CrossRef] [PubMed]
6. Lee, K.Y.; Mooney, D.J. Alginate: Properties and biomedical applications. *Prog. Polym. Sci.* **2012**, *37*, 106–126. [CrossRef] [PubMed]
7. Rowley, J.A.; Madlambayan, G.; Mooney, D.J. Alginate hydrogels as synthetic extracellular matrix materials. *Biomaterials* **1999**, *20*, 45–53. [CrossRef] [PubMed]
8. Kwon, M.Y.; Wang, C.; Galarraga, J.H.; Puré, E.; Han, L.; Burdick, J.A. Influence of hyaluronic acid modification on CD44 binding towards the design of hydrogel biomaterials. *Biomaterials* **2019**, *222*, 119451. [CrossRef] [PubMed]
9. Bouhadir, K.; Lee, K.; Alsberg, E.; Damm, K.; Anderson, K.; Mooney, D. Degradation of Partially Oxidized Alginate and Its Potential Application for Tissue Engineering. *Biotechnol. Prog.* **2001**, *17*, 945–950. [CrossRef] [PubMed]
10. Neves, M.I.; Magalhães, M.V.; Bidarra, S.J.; Moroni, L.; Barrias, C.C. Versatile click alginate hydrogels with protease-sensitive domains as cell responsive/instructive 3D microenvironments. *Carbohydr. Polym.* **2023**, *320*, 121226. [CrossRef] [PubMed]
11. Gori, M.; Vadalà, G.; Giannitelli, S.M.; Denaro, V.; Di Pino, G. Biomedical and Tissue Engineering Strategies to Control Foreign Body Reaction to Invasive Neural Electrodes. *Front. Bioeng. Biotechnol.* **2021**, *9*, 659033. [CrossRef] [PubMed]
12. Karakaya, E.; Schöbel, L.; Zhong, Y.; Hazur, J.; Heid, S.; Forster, L.; Teßmar, J.; Boccaccini, A.R.; Detsch, R. How to Determine a Suitable Alginate for Biofabrication Approaches using an Extensive Alginate Library? *Biomacromolecules* **2023**, *24*, 2982–2997. [CrossRef] [PubMed]
13. Dornish, M.; Kaplan, D.; Skaugrud, O. Standards and guidelines for biopolymers in tissue-engineered medical products: ASTM alginate and chitosan standard guides. *Ann. N. Y. Acad. Sci.* **2001**, *944*, 388–397. [CrossRef] [PubMed]
14. Zimmermann, H.; Zimmermann, D.; Reuss, R.; Feilen, P.J.; Manz, B.; Katsen, A.; Weber, M.; Ihmig, F.R.; Ehrhart, F.; Geßner, P.; et al. Towards a medically approved technology for alginate-based microcapsules allowing long-term immunoisolated transplantation. *J. Mater. Sci. Mater. Med.* **2005**, *16*, 491–501. [CrossRef] [PubMed]
15. Agarwal, T.; Onesto, V.; Banerjee, D.; Guo, S.; Polini, A.; Vogt, C.; Viswanath, A.; Esworthy, T.; Cui, H.; O'donnell, A.; et al. 3D bioprinting in tissue engineering: Current state-of-the-art and challenges towards system standardization and clinical translation. *Biofabrication* **2025**, *17*, 042003. [CrossRef] [PubMed]
16. Schwab, A.; Levato, R.; D'Este, M.; Piluso, S.; Eglin, D.; Malda, J. Printability and Shape Fidelity of Bioinks in 3D Bioprinting. *Chem. Rev.* **2020**, *120*, 11028–11055. [CrossRef] [PubMed]
17. Teixeira, M.C.; Lameirinhas, N.S.; Carvalho, J.P.F.; Silvestre, A.J.D.; Vilela, C.; Freire, C.S.R. A Guide to Polysaccharide-Based Hydrogel Bioinks for 3D Bioprinting Applications. *Int. J. Mol. Sci.* **2022**, *23*, 6564. [CrossRef] [PubMed]
18. Lim, K.S.; Galarraga, J.H.; Cui, X.; Lindberg, G.C.J.; Burdick, J.A.; Woodfield, T.B.F. Fundamentals and Applications of Photo-Cross-Linking in Bioprinting. *Chem. Rev.* **2020**, *120*, 10662–10694. [CrossRef] [PubMed]
19. Bernal, P.N.; Delrot, P.; Loterie, D.; Li, Y.; Malda, J.; Moser, C.; Levato, R. Volumetric Bioprinting of Complex Living-Tissue Constructs within Seconds. *Adv. Mater.* **2019**, *31*, 1904209. [CrossRef] [PubMed]
20. Bernal, P.N.; Bouwmeester, M.; Madrid-Wolff, J.; Falandt, M.; Florczak, S.; Rodriguez, N.G.; Li, Y.; Größbacher, G.; Samsom, R.; van Wolferen, M.; et al. Volumetric Bioprinting of Organoids and Optically Tuned Hydrogels to Build Liver-Like Metabolic Biofactories. *Adv. Mater.* **2022**, *34*, e2110054. [CrossRef] [PubMed]
21. Manzoli, S.; Merotto, E.; Piccoli, M.; Gobbo, P.; Todros, S.; Pavan, P.G. An Overview of 3D Bioprinting Impact on Cell Viability: From Damage Assessment to Protection Solutions. *J. Funct. Biomater.* **2025**, *16*, 436. [CrossRef] [PubMed]
22. Chand, R.; Muhire, B.S.; Vijayavenkataraman, S. Computational Fluid Dynamics Assessment of the Effect of Bioprinting Parameters in Extrusion Bioprinting. *Int. J. Bioprint.* **2022**, *8*, 545. [CrossRef] [PubMed]
23. Ouyang, L.; Yao, R.; Zhao, Y.; Sun, W. Effect of bioink properties on printability and cell viability for 3D bioplotting of embryonic stem cells. *Biofabrication* **2016**, *8*, 035020. [CrossRef] [PubMed]
24. Distler, T.; Solisito, A.A.; Schneidereit, D.; Friedrich, O.; Detsch, R.; Boccaccini, A.R. 3D printed oxidized alginate-gelatin bioink provides guidance for C2C12 muscle precursor cell orientation and differentiation via shear stress during bioprinting. *Biofabrication* **2020**, *12*, 045005. [CrossRef] [PubMed]

25. Markstedt, K.; Mantas, A.; Tournier, I.; Martínez Ávila, H.; Hägg, D.; Gatenholm, P. 3D Bioprinting Human Chondrocytes with Nanocellulose-Alginate Bioink for Cartilage Tissue Engineering Applications. *Biomacromolecules* **2015**, *16*, 1489–1496. [CrossRef] [PubMed]
26. Hinton, T.J.; Jallerat, Q.; Palchesko, R.N.; Park, J.H.; Grodzicki, M.S.; Shue, H.J.; Ramadan, M.H.; Hudson, A.R.; Feinberg, A.W. Three-dimensional printing of complex biological structures by freeform reversible embedding of suspended hydrogels. *Sci. Adv.* **2015**, *1*, e1500758. [CrossRef] [PubMed]
27. Mirdamadi, E.; Tashman, J.W.; Shiwarski, D.J.; Palchesko, R.N.; Feinberg, A.W. FRESH 3D Bioprinting a Full-Size Model of the Human Heart. *ACS Biomater. Sci. Eng.* **2020**, *6*, 6453–6459. [CrossRef] [PubMed]
28. Banigo, A.T.; Nauta, L.; Zoetebier, B.; Karperien, M. Coaxial Bioprinting of Enzymatically Crosslinkable Hyaluronic Acid-Tyramine Bioinks for Tissue Regeneration. *Polymers* **2024**, *16*, 2470. [CrossRef] [PubMed]
29. Zhang, J.; Suttapreyasri, S.; Leethanakul, C.; Samruajbenjakun, B. Fabrication of vascularized tissue-engineered bone models using triaxial bioprinting. *J. Biomed. Mater. Res. Part A* **2024**, *112*, 1093–1106. [CrossRef] [PubMed]
30. Yogeshwaran, S.; Goodarzi Hosseinabadi, H.; Gendy, D.E.; Miri, A.K. Design considerations and biomaterials selection in embedded extrusion 3D bioprinting. *Biomater. Sci.* **2024**, *12*, 4506–4518. [CrossRef] [PubMed]
31. Zeng, X.; Meng, Z.; He, J.; Mao, M.; Li, X.; Chen, P.; Fan, J.; Li, D. Embedded bioprinting for designer 3D tissue constructs with complex structural organization. *Acta Biomater.* **2022**, *140*, 1–22. [CrossRef] [PubMed]
32. McCormack, A.; Porcza, L.M.; Leslie, N.R.; Melchels, F.P.W. Gellan gum-based granular gels as suspension media for biofabrication. *PLoS ONE* **2024**, *19*, e0312726. [CrossRef] [PubMed]
33. Lv, W.; Naren, T.; Aazmi, A.; Yu, H.; Wang, Y.; Lee, J.Y.; Yu, M.; Jia, J.; Jiang, X.; Yang, H.; et al. Engineered Perfusable Hepatic Fibrosis Model via Embedded Sacrificial Bioprinting Recapitulates Stiffness-Driven Fibrogenesis. *Adv. Mater.* **2026**, *38*, e13401. [CrossRef] [PubMed]
34. Blaeser, A.; Duarte Campos, D.F.; Puster, U.; Richtering, W.; Stevens, M.M.; Fischer, H. Controlling Shear Stress in 3D Bioprinting is a Key Factor to Balance Printing Resolution and Stem Cell Integrity. *Adv. Healthc. Mater.* **2016**, *5*, 326–333. [CrossRef] [PubMed]
35. Gudapati, H.; Yan, J.; Huang, Y.; Chrisey, D.B. Alginate gelation-induced cell death during laser-assisted cell printing. *Biofabrication* **2014**, *6*, 035022. [CrossRef] [PubMed]
36. Steudter, T.; Lam, T.; Pirmahboub, H.; Stoppel, C.; Kloke, L.; Pearson, S.; del Campo, A. A Comparative Study between Thiol-Ene and Acrylate Photocrosslinkable Hyaluronic Acid Hydrogel Inks for Digital Light Processing. *Macromol. Biosci.* **2025**, *25*, e2400535. [CrossRef] [PubMed]
37. Feng, Z.; Li, J.; Zhou, D.; Song, H.; Lv, J.; Bai, W. A novel photocurable pullulan-based bioink for digital light processing 3D printing. *Int. J. Bioprint.* **2023**, *9*, 657. [CrossRef] [PubMed]
38. Kumari, S.; Mondal, P.; Chatterjee, K. Digital light processing-based 3D bioprinting of κ-carrageenan hydrogels for engineering cell-loaded tissue scaffolds. *Carbohydr. Polym.* **2022**, *290*, 119508. [CrossRef] [PubMed]
39. Pahlevanzadeh, F.; Emadi, R.; Valiani, A.; Kharaziha, M.; Poursamar, S.A.; Bakhsheshi-Rad, H.R.; Ismail, A.F.; RamaKrishna, S.; Berto, F. Three-Dimensional Printing Constructs Based on the Chitosan for Tissue Regeneration: State of the Art, Developing Directions and Prospect Trends. *Materials* **2020**, *13*, 2663. [CrossRef] [PubMed]
40. Graham, S.; Marina, P.F.; Blencowe, A. Thermoresponsive polysaccharides and their thermoreversible physical hydrogel networks. *Carbohydr. Polym.* **2019**, *207*, 143–159. [CrossRef] [PubMed]
41. Wu, S.; Xiao, R.; Wu, Y.; Xu, L. Advances in tissue engineering of gellan gum-based hydrogels. *Carbohydr. Polym.* **2024**, *324*, 121484. [CrossRef] [PubMed]
42. Merli, M.; Sardelli, L.; Baranzini, N.; Grimaldi, A.; Jacchetti, E.; Raimondi, M.T.; Briatico-Vangosa, F.; Petrini, P.; Tunesi, M. Pectin-based bioinks for 3D models of neural tissue produced by a pH-controlled kinetics. *Front. Bioeng. Biotechnol.* **2022**, *10*, 1032542. [CrossRef] [PubMed]
43. Lameirinhas, N.S.; Teixeira, M.C.; Carvalho, J.P.F.; Valente, B.F.A.; Pinto, R.J.B.; Oliveira, H.; Luís, J.L.; Pires, L.; Oliveira, J.M.; Vilela, C.; et al. Nanofibrillated cellulose/gellan gum hydrogel-based bioinks for 3D bioprinting of skin cells. *Int. J. Biol. Macromol.* **2023**, *229*, 849–860. [CrossRef] [PubMed]
44. Paoletti, L.; Baschieri, F.; Migliorini, C.; Di Meo, C.; Monasson, O.; Peroni, E.; Matricardi, P. 3D printing of gellan-dextran methacrylate IPNs in glycerol and their bioadhesion by RGD derivatives. *J. Biomed. Mater. Res. Part A* **2024**, *112*, 1107–1123. [CrossRef] [PubMed]
45. Jessop, Z.M.; Al-Sabah, A.; Gao, N.; Kyle, S.; Thomas, B.; Badiei, N.; Hawkins, K.; Whitaker, I.S. Printability of pulp derived crystal, fibril and blend nanocellulose-alginate bioinks for extrusion 3D bioprinting. *Biofabrication* **2019**, *11*, 045006. [CrossRef] [PubMed]
46. Pang, Y.; Wang, X.; Zhang, H.; Li, X.; Lin, M.; Cheng, L.; Yang, Y.-W. RGD-grafted dextran methacrylate hydrogel incorporating osteogenic peptide and Mn(3)O(4) nanozymes for enhanced bone defect healing. *Mater. Today Bio* **2025**, *35*, 102436. [CrossRef] [PubMed]

47. Bhattacharyya, A.; Ham, H.W.; Sonh, J.; Gunbayar, M.; Jeffy, R.; Nagarajan, R.; Khatun, M.R.; Noh, I. 3D bioprinting of complex tissue scaffolds with in situ homogeneously mixed alginate-chitosan-kaolin bioink using advanced portable biopen. *Carbohydr. Polym.* **2023**, *317*, 121046. [CrossRef] [PubMed]
48. Ren, P.; Yang, L.; Wei, D.; Liang, M.; Xu, L.; Zhang, T.; Hu, W.; Zhang, Z.; Zhang, Q. Alginate/polyacrylamide host-guest supramolecular hydrogels with enhanced adhesion. *Int. J. Biol. Macromol.* **2023**, *242*, 124885. [CrossRef] [PubMed]
49. Jiang, T.; Yang, Y.; Lin, Z.; Hong, Y.; Luo, Z. Modified Polysaccharides: Potential Biomaterials for Bioprinting. *J. Funct. Biomater.* **2025**, *16*, 338. [CrossRef] [PubMed]
50. Mihajlovic, M.; Rikkers, M.; Mihajlovic, M.; Viola, M.; Schuiringa, G.; Ilochonwu, B.C.; Masereeuw, R.; Vonk, L.; Malda, J.; Ito, K.; et al. Viscoelastic Chondroitin Sulfate and Hyaluronic Acid Double-Network Hydrogels with Reversible Cross-Links. *Biomacromolecules* **2022**, *23*, 1350–1365. [CrossRef] [PubMed]
51. Singh, R.S.; Kaur, N.; Rana, V.; Kennedy, J.F. Recent insights on applications of pullulan in tissue engineering. *Carbohydr. Polym.* **2016**, *153*, 455–462. [CrossRef] [PubMed]
52. Zhuang, P.; Greenberg, Z.; He, M. Biologically enhanced starch bio-ink for promoting 3D cell growth. *Adv. Mater. Technol.* **2021**, *6*, 2100551. [CrossRef] [PubMed]
53. Faber, J.; Hinrichsen, J.; Soufivand, A.A.; Lu, H.H.; Rosenberger, T.; Karakaya, E.; Detsch, R.; Boccaccini, A.R.; Budday, S. Tuning the mechanical properties of alginate dialdehyde–gelatin (ADA–GEL) bioinks for bioprinting approaches by varying the degree of oxidation. *J. Mech. Behav. Biomed. Mater.* **2025**, *163*, 106871. [CrossRef] [PubMed]
54. Kim, E.; Seok, J.M.; Bae, S.B.; Park, S.A.; Park, W.H. Silk Fibroin Enhances Cytocompatibilty and Dimensional Stability of Alginate Hydrogels for Light-Based Three-Dimensional Bioprinting. *Biomacromolecules* **2021**, *22*, 1921–1931. [CrossRef] [PubMed]
55. Moheimani, H.; Stealey, S.; Neal, S.; Ferchichi, E.; Zhang, J.; Foston, M.; Setton, L.A.; Genin, G.M.; Huebsch, N.; Zustiak, S.P. Tunable Viscoelasticity of Alginate Hydrogels via Serial Autoclaving. *Adv. Healthc. Mater.* **2024**, *13*, e2401550. [CrossRef] [PubMed]
56. Zhang, W.; Kuss, M.; Yan, Y.; Shi, W. Dynamic Alginate Hydrogel as an Antioxidative Bioink for Bioprinting. *Gels* **2023**, *9*, 312. [CrossRef] [PubMed]
57. Ouyang, L.; Highley, C.B.; Rodell, C.B.; Sun, W.; Burdick, J.A. 3D Printing of Shear-Thinning Hyaluronic Acid Hydrogels with Secondary Cross-Linking. *ACS Biomater. Sci. Eng.* **2016**, *2*, 1743–1751. [CrossRef] [PubMed]
58. Highley, C.B.; Rodell, C.B.; Burdick, J.A. Direct 3D Printing of Shear-Thinning Hydrogels into Self-Healing Hydrogels. *Adv. Mater.* **2015**, *27*, 5075–5079. [CrossRef] [PubMed]
59. Hossain Rakin, R.; Kumar, H.; Rajeev, A.; Natale, G.; Menard, F.; Li, I.T.S.; Kim, K. Tunable metacrylated hyaluronic acid-based hybrid bioinks for stereolithography 3D bioprinting. *Biofabrication* **2021**, *13*, 044109. [CrossRef] [PubMed]
60. Kesti, M.; Muller, M.; Becher, J.; Schnabelrauch, M.; D'Este, M.; Eglin, D.; Zenobi-Wong, M. A versatile bioink for three-dimensional printing of cellular scaffolds based on thermally and photo-triggered tandem gelation. *Acta Biomater.* **2015**, *11*, 162–172. [CrossRef] [PubMed]
61. Xiao, X.; Yang, Y.; Lai, Y.; Huang, Z.; Li, C.; Yang, S.; Niu, C.; Yang, L.; Feng, L. Customization of an Ultrafast Thiol–Norbornene Photo-Cross-Linkable Hyaluronic Acid–Gelatin Bioink for Extrusion-Based 3D Bioprinting. *Biomacromolecules* **2023**, *24*, 5414–5427. [CrossRef] [PubMed]
62. LeSavage, B.L.; Zhang, D.; Huerta-López, C.; Gilchrist, A.E.; Krajina, B.A.; Karlsson, K.; Smith, A.R.; Karagyozova, K.; Klett, K.C.; Huang, M.S.; et al. Engineered matrices reveal stiffness-mediated chemoresistance in patient-derived pancreatic cancer organoids. *Nat. Mater.* **2024**, *23*, 1138–1149. [CrossRef] [PubMed]
63. Lisková, J.; Bačaková, L.; Skwarczyńska, A.L.; Musial, O.; Bliznuk, V.; De Schamphelaere, K.; Modrzejewska, Z.; Douglas, T.E. Development of thermosensitive hydrogels of chitosan, sodium and magnesium glycerophosphate for bone regeneration applications. *J. Funct. Biomater.* **2015**, *6*, 192–203. [CrossRef] [PubMed]
64. Maiz-Fernández, S.; Pérez-Álvarez, L.; Silván, U.; Vilas-Vilela, J.L.; Lanceros-Méndez, S. pH-Induced 3D Printable Chitosan Hydrogels for Soft Actuation. *Polymers* **2022**, *14*, 650. [CrossRef] [PubMed]
65. Khoshnood, N.; Frampton, J.P.; Zamanian, A. 3D bioprinted alginate/chitosan-based sandwich-structured wound dressing with dual-drug release for enhanced skin regeneration. *Int. J. Biol. Macromol.* **2025**, *332*, 148428. [CrossRef] [PubMed]
66. Wattanaeabpun, S.; Charoenthanakitkul, D.; Ariyachet, C.; Aumnate, C.; Hongrattanavichit, I. Influence of pre-printing aging time on the printability and performance of chitosan–polyacrylic acid double-network hydrogels for skin graft application. *Int. J. Biol. Macromol.* **2026**, *342*, 150401. [CrossRef] [PubMed]
67. Chimene, D.; Miller, L.; Cross, L.M.; Jaiswal, M.K.; Singh, I.; Gaharwar, A.K. Nanoengineered Osteoinductive Bioink for 3D Bioprinting Bone Tissue. *ACS Appl. Mater. Interfaces* **2020**, *12*, 15976–15988. [CrossRef] [PubMed]
68. Butler, H.M.; Naseri, E.; MacDonald, D.S.; Tasker, R.A.; Ahmadi, A. Investigation of rheology, printability, and biocompatibility of N,O-carboxymethyl chitosan and agarose bioinks for 3D bioprinting of neuron cells. *Materialia* **2021**, *18*, 101169. [CrossRef]
69. Shin, J.Y.; Yeo, Y.H.; Jeong, J.E.; Park, S.A.; Park, W.H. Dual-crosslinked methylcellulose hydrogels for 3D bioprinting applications. *Carbohydr. Polym.* **2020**, *238*, 116192. [CrossRef] [PubMed]

70. Nguyen, D.; Hägg, D.A.; Forsman, A.; Ekholm, J.; Nimkingratana, P.; Brantsing, C.; Kalogeropoulos, T.; Zaunz, S.; Concaro, S.; Brittberg, M.; et al. Cartilage Tissue Engineering by the 3D Bioprinting of iPS Cells in a Nanocellulose/Alginate Bioink. *Sci. Rep.* **2017**, *7*, 658. [CrossRef] [PubMed]
71. Apelgren, P.; Karabulut, E.; Amoroso, M.; Mantas, A.; Martínez Ávila, H.; Kölby, L.; Kondo, T.; Toriz, G.; Gatenholm, P. In Vivo Human Cartilage Formation in Three-Dimensional Bioprinted Constructs with a Novel Bacterial Nanocellulose Bioink. *ACS Biomater. Sci. Eng.* **2019**, *5*, 2482–2490. [CrossRef] [PubMed]
72. Sathish, P.B.; Gayathri, S.; Priyanka, J.; Shalini, M.; Narmadha, R.; Shankar, K.G.; Selvakumar, R. Tricomposite gelatin-carboxymethylcellulose-alginate bioink for direct and indirect 3D printing of human knee meniscal scaffold. *Int. J. Biol. Macromol.* **2022**, *195*, 179–189. [CrossRef] [PubMed]
73. Budharaju, H.; Chandrababu, H.; Zennifer, A.; Chellappan, D.; Sethuraman, S.; Sundaramurthi, D. Tuning thermoresponsive properties of carboxymethyl cellulose (CMC)–agarose composite bioinks to fabricate complex 3D constructs for regenerative medicine. *Int. J. Biol. Macromol.* **2024**, *260*, 129443. [CrossRef] [PubMed]
74. Lafuente-Merchan, M.; Ruiz-Alonso, S.; Espona-Noguera, A.; Galvez-Martin, P.; López-Ruiz, E.; Marchal, J.A.; López-Donaire, M.; Zabala, A.; Ciriza, J.; Saenz-Del-Burgo, L.; et al. Development, characterization and sterilisation of Nanocellulose-alginate-(hyaluronic acid)- bioinks and 3D bioprinted scaffolds for tissue engineering. *Mater. Sci. Eng. C* **2021**, *126*, 112160. [CrossRef] [PubMed]
75. Apelgren, P.; Sämfors, S.; Säljö, K.; Mölne, J.; Gatenholm, P.; Troedsson, C.; Thompson, E.M.; Kölby, L. Biomaterial and biocompatibility evaluation of tunicate nanocellulose for tissue engineering. *Biomater. Adv.* **2022**, *137*, 212828. [CrossRef] [PubMed]
76. Cernencu, A.I.; Ioniță, M. The current state of the art in gellan-based printing inks in tissue engineering. *Carbohydr. Polym.* **2023**, *309*, 120676. [CrossRef] [PubMed]
77. Bagewadi, S.; Rajendran, M.; Ganapathisankarakrishnan, A.; Budharaju, H.; Sethuraman, S.; Sundaramurthi, D. Preparation of thermoresponsive & enzymatically crosslinkable gelatin-gellan gum bioink: A protein-polysaccharide hydrogel for 3D bioprinting of complex soft tissues. *Int. J. Biol. Macromol.* **2025**, *295*, 139563. [CrossRef] [PubMed]
78. Bonifacio, M.A.; Cometa, S.; Cochis, A.; Scalzone, A.; Gentile, P.; Scalia, A.C.; Rimondini, L.; Mastrorilli, P.; De Giglio, E. A bioprintable gellan gum/lignin hydrogel: A smart and sustainable route for cartilage regeneration. *Int. J. Biol. Macromol.* **2022**, *216*, 336–346. [CrossRef] [PubMed]
79. Dravid, A.; McCaughey-Chapman, A.; Raos, B.; O'Carroll, S.J.; Connor, B.; Svirskis, D. Development of agarose-gelatin bioinks for extrusion-based bioprinting and cell encapsulation. *Biomed. Mater.* **2022**, *17*, 055001. [CrossRef] [PubMed]
80. Mukundan, L.M.; Rajasekaran, R.; Das, S.; Seesala, V.S.; Ganguly, D.; Kumar, N.; Dhara, S.; Chattopadhyay, S. Tailoring of agarose hydrogel to modulate its 3D bioprintability and mechanical properties for stem cell mediated bone tissue engineering. *Int. J. Biol. Macromol.* **2025**, *309*, 142795. [CrossRef] [PubMed]
81. Liu, Q.; Yang, J.; Wang, Y.; Wu, T.; Liang, Y.; Deng, K.; Luan, G.; Chen, Y.; Huang, Z.; Yue, K. Direct 3D Bioprinting of Tough and Antifatigue Cell-Laden Constructs Enabled by a Self-Healing Hydrogel Bioink. *Biomacromolecules* **2023**, *24*, 2549–2562. [CrossRef] [PubMed]
82. Costantini, M.; Idaszek, J.; Szöke, K.; Jaroszewicz, J.; Dentini, M.; Barbetta, A.; Brinchmann, J.E.; Święszkowski, W. 3D bioprinting of BM-MSCs-loaded ECM biomimetic hydrogels for in vitro neocartilage formation. *Biofabrication* **2016**, *8*, 035002. [CrossRef] [PubMed]
83. Olate-Moya, F.; Rubí-Sans, G.; Engel, E.; Mateos-Timoneda, M.Á.; Palza, H. 3D Bioprinting of Biomimetic Alginate/Gelatin/Chondroitin Sulfate Hydrogel Nanocomposites for Intrinsically Chondrogenic Differentiation of Human Mesenchymal Stem Cells. *Biomacromolecules* **2024**, *25*, 3312–3324. [CrossRef] [PubMed]
84. Marques, D.M.C.; Silva, J.C.; Serro, A.P.; Cabral, J.M.S.; Sanjuan-Alberte, P.; Ferreira, F.C. 3D Bioprinting of Novel κ-Carrageenan Bioinks: An Algae-Derived Polysaccharide. *Bioengineering* **2022**, *9*, 109. [CrossRef] [PubMed]
85. Lim, W.; Kim, G.J.; Kim, H.W.; Lee, J.; Zhang, X.; Kang, M.G.; Seo, J.W.; Cha, J.M.; Park, H.J.; Lee, M.-Y.; et al. Kappa-Carrageenan-Based Dual Crosslinkable Bioink for Extrusion Type Bioprinting. *Polymers* **2020**, *12*, 2377. [CrossRef] [PubMed]
86. Kim, M.H.; Lee, Y.W.; Jung, W.K.; Oh, J.; Nam, S.Y. Enhanced rheological behaviors of alginate hydrogels with carrageenan for extrusion-based bioprinting. *J. Mech. Behav. Biomed. Mater.* **2019**, *98*, 187–194. [CrossRef] [PubMed]
87. Yilmaz-Aykut, D.; Torkay, G.; Kasgoz, A.; Shin, S.R.; Bal-Ozturk, A.; Deligoz, H. Injectable and self-healing dual crosslinked gelatin/kappa-carrageenan methacryloyl hybrid hydrogels via host-guest supramolecular interaction for wound healing. *J. Biomed. Mater. Res. Part B* **2023**, *111*, 1921–1937. [CrossRef] [PubMed]
88. Pitton, M.; Fiorati, A.; Buscemi, S.; Melone, L.; Farè, S.; Contessi Negrini, N. 3D Bioprinting of Pectin-Cellulose Nanofibers Multicomponent Bioinks. *Front. Bioeng. Biotechnol.* **2021**, *9*, 732689. [CrossRef] [PubMed]
89. Mubarok, W.; Zhang, C.; Sakai, S. 3D Bioprinting of Sugar Beet Pectin through Horseradish Peroxidase-Catalyzed Cross-Linking. *ACS Appl. Bio Mater.* **2024**, *7*, 3506–3514. [CrossRef] [PubMed]

90. Elangwe, C.N.; Morozkina, S.N.; Olekhnovich, R.O.; Polyakova, V.O.; Krasichkov, A.; Yablonskiy, P.K.; Uspenskaya, M.V. Pullulan-Based Hydrogels in Wound Healing and Skin Tissue Engineering Applications: A Review. *Int. J. Mol. Sci.* **2023**, *24*, 4962. [CrossRef] [PubMed]
91. Zhao, Y.; Li, R.; Liu, Y.; Song, L.; Gao, Z.; Li, Z.; Peng, X.; Wang, P. An injectable, self-healable, antibacterial, and pro-healing oxidized pullulan polysaccharide/carboxymethyl chitosan hydrogel for early protection of open abdominal wounds. *Int. J. Biol. Macromol.* **2023**, *250*, 126282. [CrossRef] [PubMed]
92. Zhou, X.; Wu, S.; Liu, P.; Wang, L.; Xie, F. Hybrid bioink of methyacrylated starch with minimal methacrylated chitosan enables high-precision 3D printing for complex tissue scaffolds. *Carbohydr. Polym.* **2025**, *367*, 124023. [CrossRef] [PubMed]
93. Zennifer, A.; Manivannan, S.; Sethuraman, S.; Kumbar, S.G.; Sundaramurthi, D. 3D bioprinting and photocrosslinking: Emerging strategies & future perspectives. *Biomater. Adv.* **2022**, *134*, 112576. [CrossRef] [PubMed]
94. Lim, K.S.; Klotz, B.J.; Lindberg, G.C.J.; Melchels, F.P.W.; Hooper, G.J.; Malda, J.; Gawlitta, D.; Woodfield, T.B.F. Visible Light Cross-Linking of Gelatin Hydrogels Offers an Enhanced Cell Microenvironment with Improved Light Penetration Depth. *Macromol. Biosci.* **2019**, *19*, e1900098. [CrossRef] [PubMed]
95. Kim, M.H.; Lin, C.C. Poly(ethylene glycol)–Norbornene as a Photoclick Bioink for Digital Light Processing 3D Bioprinting. *ACS Appl. Mater. Interfaces* **2023**, *15*, 2737–2746. [CrossRef] [PubMed]
96. Mueller, E.; Poulin, I.; Bodnaryk, W.J.; Hoare, T. Click Chemistry Hydrogels for Extrusion Bioprinting: Progress, Challenges, and Opportunities. *Biomacromolecules* **2022**, *23*, 619–640. [CrossRef] [PubMed]
97. Li, S.; Pei, M.; Wan, T.; Yang, H.; Gu, S.; Tao, Y.; Liu, X.; Zhou, Y.; Xu, W.; Xiao, P. Self-healing hyaluronic acid hydrogels based on dynamic Schiff base linkages as biomaterials. *Carbohydr. Polym.* **2020**, *250*, 116922. [CrossRef] [PubMed]
98. Morgan, F.L.C.; Fernández-Pérez, J.; Moroni, L.; Baker, M.B. Tuning Hydrogels by Mixing Dynamic Cross-Linkers: Enabling Cell-Instructive Hydrogels and Advanced Bioinks. *Adv. Healthc. Mater.* **2022**, *11*, e2101576. [CrossRef] [PubMed]
99. Wang, L.; Liu, Y.; Zhang, Y.; Sun, Q.; Wang, X.; Li, Q.; Li, X. Dual-crosslinkable alginate hydrogel with dynamic viscoelasticity for chondrogenic and osteogenic differentiation of mesenchymal stem cells. *Int. J. Biol. Macromol.* **2025**, *307*, 142346. [CrossRef] [PubMed]
100. Budharaju, H.; Sundaramurthi, D.; Sethuraman, S. Efficient dual crosslinking of protein–in–polysaccharide bioink for biofabrication of cardiac tissue constructs. *Biomater. Adv.* **2023**, *152*, 213486. [CrossRef] [PubMed]
101. Shan, J.; Kong, Z.; Wang, X. Formation of Stable Vascular Networks by 3D Coaxial Printing and Schiff-Based Reaction. *Gels* **2024**, *10*, 366. [CrossRef] [PubMed]
102. Paxton, N.; Smolan, W.; Böck, T.; Melchels, F.; Groll, J.; Jungst, T. Proposal to assess printability of bioinks for extrusion-based bioprinting and evaluation of rheological properties governing bioprintability. *Biofabrication* **2017**, *9*, 044107. [CrossRef] [PubMed]
103. Ahmad, S.; Alam, H.; Thareja, P. 3D printing of hydrogels: A synergistic approach of rheology and computational fluid dynamics (CFD) modeling. *RSC Adv.* **2025**, *15*, 39369–39390. [CrossRef] [PubMed]
104. Ribeiro, A.; Blokzijl, M.M.; Levato, R.; Visser, C.W.; Castilho, M.; Hennink, W.E.; Vermonden, T.; Malda, J. Assessing bioink shape fidelity to aid material development in 3D bioprinting. *Biofabrication* **2017**, *10*, 014102. [CrossRef] [PubMed]
105. Gillispie, G.J.; Copus, J.; Uzun-Per, M.; Yoo, J.J.; Atala, A.; Niazi, M.K.K.; Lee, S.J. The correlation between rheological properties and extrusion-based printability in bioink artifact quantification. *Mater. Des.* **2023**, *233*, 112237. [CrossRef] [PubMed]
106. Kiyotake, E.A.; Douglas, A.W.; Thomas, E.E.; Nimmo, S.L.; Detamore, M.S. Development and quantitative characterization of the precursor rheology of hyaluronic acid hydrogels for bioprinting. *Acta Biomater.* **2019**, *95*, 176–187. [CrossRef] [PubMed]
107. Yu, S.; Luo, Y.; Chen, S.; Fan, J.; Zhang, H. Quantitative Assessment of Hydrogel Printability in Extrusion Bioprinting. *Gels* **2026**, *12*, 189. [CrossRef] [PubMed]
108. Zhang, C.; Elvitigala, K.C.M.L.; Sakai, S. AI-powered printability evaluation framework for 3D bioprinting using Hausdorff distance metrics. *Biofabrication* **2026**, *18*, 015015. [CrossRef] [PubMed]
109. O'Connell, C.D.; Dalton, P.D.; Hutmacher, D.W. Why bioprinting in regenerative medicine should adopt a rational technology readiness assessment. *Trends Biotechnol.* **2024**, *42*, 1218–1229. [CrossRef] [PubMed]
110. Chaudhuri, O.; Gu, L.; Klumpers, D.; Darnell, M.; Bencherif, S.A.; Weaver, J.C.; Huebsch, N.; Lee, H.-P.; Lippens, E.; Duda, G.N.; et al. Hydrogels with tunable stress relaxation regulate stem cell fate and activity. *Nat. Mater.* **2016**, *15*, 326–334. [CrossRef] [PubMed]
111. Lin, C.; He, Y.; Feng, Q.; Xu, K.; Chen, Z.; Tao, B.; Li, X.; Xia, Z.; Jiang, H.; Cai, K. Self-renewal or quiescence? Orchestrating the fate of mesenchymal stem cells by matrix viscoelasticity via PI3K/Akt-CDK1 pathway. *Biomaterials* **2021**, *279*, 121235. [CrossRef] [PubMed]
112. Daly, A.C.; Freeman, F.E.; Gonzalez-Fernandez, T.; Critchley, S.E.; Nulty, J.; Kelly, D.J. 3D Bioprinting for Cartilage and Osteochondral Tissue Engineering. *Adv. Healthc. Mater.* **2017**, *6*, 1700298. [CrossRef] [PubMed]
113. Idaszek, J.; Costantini, M.; Karlsen, T.A.; Jaroszewicz, J.; Colosi, C.; Testa, S.; Fornetti, E.; Bernardini, S.; Seta, M.; Kasarełło, K.; et al. 3D bioprinting of hydrogel constructs with cell and material gradients for the regeneration of full-thickness chondral defect using a microfluidic printing head. *Biofabrication* **2019**, *11*, 044101. [CrossRef] [PubMed]

114. Korkeamäki, J.T.; Rashad, A.; Ojansivu, M.; Karvinen, J.; Koivisto, J.T.; Syverud, K.; Kellomäki, M.; Miettinen, S.; Mustafa, K. Systematic development and bioprinting of novel nanostructured multi-material bioinks for bone tissue engineering. *Biofabrication* **2025**, *17*, 025005. [CrossRef] [PubMed]
115. Wang, C.; Hu, C.; Cheng, H.; Qi, W.; Wang, L.; Wu, T.; Wu, J.; Cui, X.; Xu, J.; Pan, H.; et al. A Programmable Handheld Extrusion-Based Bioprinting Platform for In Situ Skin Wounds Dressing: Balance Mobility and Customizability. *Adv. Sci.* **2024**, *11*, e2405823. [CrossRef] [PubMed]
116. Samandari, M.; Mostafavi, A.; Quint, J.; Memić, A.; Tamayol, A. In situ bioprinting: Intraoperative implementation of regenerative medicine. *Trends Biotechnol.* **2022**, *40*, 1229–1247. [CrossRef] [PubMed]
117. Albouy, M.; Desanlis, A.; Brosset, S.; Auxenfans, C.; Courtial, E.J.; Eli, K.; Cambron, S.; Palmer, J.M.; Vidal, L.; Thépot, A.; et al. A Preliminary Study for an Intraoperative 3D Bioprinting Treatment of Severe Burn Injuries. *Plast. Reconstr. Surg. Glob. Open* **2022**, *10*, e4056. [CrossRef] [PubMed]
118. Zhang, T.; Sheng, S.; Cai, W.; Yang, H.; Li, J.; Niu, L.; Chen, W.; Zhang, X.; Zhou, Q.; Gao, C.; et al. 3-D bioprinted human-derived skin organoids accelerate full-thickness skin defects repair. *Bioact. Mater.* **2024**, *42*, 257–269. [CrossRef] [PubMed]
119. Yeo, M.; Sarkar, A.; Singh, Y.P.; Derman, I.D.; Datta, P.; Ozbolat, I.T. Synergistic coupling between 3D bioprinting and vascularization strategies. *Biofabrication* **2023**, *16*, 012003. [CrossRef] [PubMed]
120. Miller, J.S.; Stevens, K.R.; Yang, M.T.; Baker, B.M.; Nguyen, D.H.; Cohen, D.M.; Toro, E.; Chen, A.A.; Galie, P.A.; Yu, X.; et al. Rapid casting of patterned vascular networks for perfusable engineered three-dimensional tissues. *Nat. Mater.* **2012**, *11*, 768–774. [CrossRef] [PubMed]
121. Grigoryan, B.; Paulsen, S.J.; Corbett, D.C.; Sazer, D.W.; Fortin, C.L.; Zaita, A.J.; Greenfield, P.T.; Calafat, N.J.; Gounley, J.P.; Ta, A.H.; et al. Multivascular networks and functional intravascular topologies within biocompatible hydrogels. *Science* **2019**, *364*, 458–464. [CrossRef] [PubMed]
122. Stankey, P.P.; Kroll, K.T.; Ainscough, A.J.; Reynolds, D.S.; Elamine, A.; Fichtenkort, B.T.; Uzel, S.G.; Lewis, J.A. Embedding Biomimetic Vascular Networks via Coaxial Sacrificial Writing into Functional Tissue. *Adv. Mater.* **2024**, *36*, e2401528. [CrossRef] [PubMed]
123. Lee, A.; Hudson, A.R.; Shiwarski, D.J.; Tashman, J.W.; Hinton, T.J.; Yerneni, S.; Bliley, J.M.; Campbell, P.G.; Feinberg, A.W. 3D bioprinting of collagen to rebuild components of the human heart. *Science* **2019**, *365*, 482–487. [CrossRef] [PubMed]
124. Basara, G.; Ozcebe, S.G.; Ellis, B.W.; Zorlutuna, P. Tunable Human Myocardium Derived Decellularized Extracellular Matrix for 3D Bioprinting and Cardiac Tissue Engineering. *Gels* **2021**, *7*, 70. [CrossRef] [PubMed]
125. Kim, B.S.; Das, S.; Jang, J.; Cho, D.W. Decellularized Extracellular Matrix-based Bioinks for Engineering Tissue- and Organ-specific Microenvironments. *Chem. Rev.* **2020**, *120*, 10608–10661. [CrossRef] [PubMed]
126. Cadena, M.; Ning, L.; King, A.; Hwang, B.; Jin, L.; Serpooshan, V.; Sloan, S.A. 3D Bioprinting of Neural Tissues. *Adv. Healthc. Mater.* **2021**, *10*, e2001600. [CrossRef] [PubMed]
127. Koffler, J.; Zhu, W.; Qu, X.; Platoshyn, O.; Dulin, J.N.; Brock, J.; Graham, L.; Lu, P.; Sakamoto, J.; Marsala, M.; et al. Biomimetic 3D-printed scaffolds for spinal cord injury repair. *Nat. Med.* **2019**, *25*, 263–269. [CrossRef] [PubMed]
128. Li, G.; He, J.; Shi, J.; Li, X.; Liu, L.; Ge, X.; Chen, W.; Jia, J.; Wang, J.; Yin, M.; et al. Bioprinting functional hepatocyte organoids derived from human chemically induced pluripotent stem cells to treat liver failure. *Gut* **2025**, *74*, 1150–1164. [CrossRef] [PubMed]
129. Brassard, J.A.; Nikolaev, M.; Hübscher, T.; Hofer, M.; Lutolf, M.P. Recapitulating macro-scale tissue self-organization through organoid bioprinting. *Nat. Mater.* **2021**, *20*, 22–29. [CrossRef] [PubMed]
130. Gebeyehu, A.; Surapaneni, S.K.; Huang, J.; Mondal, A.; Wang, V.Z.; Haruna, N.F.; Bagde, A.; Arthur, P.; Kutlehria, S.; Patel, N.; et al. Polysaccharide hydrogel based 3D printed tumor models for chemotherapeutic drug screening. *Sci. Rep.* **2021**, *11*, 372. [CrossRef] [PubMed]
131. Levin, A.A.; Karalkin, P.A.; Koudan, E.V.; Senatov, F.S.; Parfenov, V.A.; Lvov, V.A.; Petrov, S.V.; Pereira, F.D.A.S.; Kovalev, A.V.; Osidak, E.O.; et al. Commercial articulated collaborative in situ 3D bioprinter for skin wound healing. *Int. J. Bioprint.* **2023**, *9*, 675. [CrossRef] [PubMed]
132. Kolesky, D.B.; Truby, R.L.; Gladman, A.S.; Busbee, T.A.; Homan, K.A.; Lewis, J.A. 3D Bioprinting of Vascularized, Heterogeneous Cell-Laden Tissue Constructs. *Adv. Mater.* **2014**, *26*, 3124–3130. [CrossRef] [PubMed]
133. Shin, Y.J.; Safina, D.; Zheng, Y.; Levenberg, S. Microvascularization in 3D Human Engineered Tissue and Organoids. *Annu. Rev. Biomed. Eng.* **2025**, *27*, 473–498. [CrossRef] [PubMed]
134. Pati, F.; Jang, J.; Ha, D.H.; Won Kim, S.; Rhie, J.W.; Shim, J.H.; Kim, D.-H.; Cho, D.-W. Printing three-dimensional tissue analogues with decellularized extracellular matrix bioink. *Nat. Commun.* **2014**, *5*, 3935. [CrossRef] [PubMed]
135. Wu, H.; Xu, F.; Jin, H.; Xue, M.; Zhang, W.; Yang, J.; Huang, J.; Jiang, Y.; Qiu, B.; Lin, B.; et al. 3D Nanofiber-Assisted Embedded Extrusion Bioprinting for Oriented Cardiac Tissue Fabrication. *ACS Biomater. Sci. Eng.* **2024**, *10*, 7256–7265. [CrossRef] [PubMed]
136. U.S. Food and Drug Administration. Pyrogen and Endotoxins Testing: Questions and Answers; Guidance for Industry (Docket FDA-2013-S-0610). Available online: https://www.fda.gov/regulatory-information/search-fda-guidance-documents/pyrogen-and-endotoxins-testing-questions-and-answers (accessed on 4 September 2026).

137. Lorson, T.; Ruopp, M.; Nadernezhad, A.; Eiber, J.; Vogel, U.; Jungst, T.; Lühmann, T. Sterilization Methods and Their Influence on Physicochemical Properties and Bioprinting of Alginate as a Bioink Component. *ACS Omega* **2020**, *5*, 6481–6486. [CrossRef] [PubMed]
138. Heinemann, C.; Buchner, F.; Lee, P.S.; Bernhardt, A.; Kruppke, B.; Wiesmann, H.P.; Hintze, V. Effects of Gamma Irradiation and Supercritical Carbon Dioxide Sterilization on Methacrylated Gelatin/Hyaluronan Hydrogels. *J. Funct. Biomater.* **2023**, *14*, 317. [CrossRef] [PubMed]
139. Zhou, Y.; Ma, Y.; Samad, A.; Wang, Z.; Gu, Z.; Shi, J.; Cui, Y.; He, Y.; Gu, Z. Effects of irradiation sterilization on the physicochemical and functional properties of commercial biomedical hydrogels. *Biomater. Sci.* **2025**, *13*, 6270–6284. [CrossRef] [PubMed]
140. Op 't Veld, R.C.; Eerden, M.; Wagener, F.A.D.T.G.; Kouwer, P.H.J.; Jansen, J.A.; Walboomers, X.F. Polyisocyanopeptide Hydrogels Are Effectively Sterilized Using Supercritical Carbon Dioxide. *Tissue Eng. Part C* **2020**, *26*, 132–141. [CrossRef] [PubMed]
141. Murphy, S.V.; De Coppi, P.; Atala, A. Opportunities and challenges of translational 3D bioprinting. *Nat. Biomed. Eng.* **2020**, *4*, 370–380. [CrossRef] [PubMed]
142. European Commission. EudraLex Volume 4—Good Manufacturing Practice (GMP) Guidelines, Part IV: Guidelines on Good Manufacturing Practice Specific to Advanced Therapy Medicinal Products. Available online: https://health.ec.europa.eu/medicinal-products/eudralex/eudralex-volume-4_en (accessed on 4 September 2026).
143. U.S. Food and Drug Administration. Technical Considerations for Additive Manufactured Medical Devices: Guidance for Industry and Food and Drug Administration Staff (Docket FDA-2016-D-1210). Available online: https://www.fda.gov/regulatory-information/search-fda-guidance-documents/technical-considerations-additive-manufactured-medical-devices (accessed on 4 September 2026).
144. U.S. Food and Drug Administration. Use of International Standard ISO 10993-1, "Biological Evaluation of Medical Devices—Part 1: Evaluation and Testing Within a Risk Management Process"; Guidance for Industry and Food and Drug Administration Staff (Docket FDA-2013-D-0350). Available online: https://www.fda.gov/regulatory-information/search-fda-guidance-documents/use-international-standard-iso-10993-1-biological-evaluation-medical-devices-part-1-evaluation-and (accessed on 4 September 2026).
145. Code of Federal Regulations, Title 21, Part 1271, Section 1271.10: Are My HCT/P's Regulated Solely Under Section 361 of the PHS Act and the Regulations in This Part, and If so What Must I Do? Electronic Code of Federal Regulations (Current). Available online: https://www.ecfr.gov/current/title-21/chapter-I/subchapter-L/part-1271/subpart-A/section-1271.10 (accessed on 4 September 2026).
146. U.S. Food and Drug Administration. Regulatory Considerations for Human Cells, Tissues, and Cellular and Tissue-Based Products: Minimal Manipulation and Homologous Use; Guidance for Industry and Food and Drug Administration Staff (Docket FDA-2017-D-6146). Available online: https://www.fda.gov/regulatory-information/search-fda-guidance-documents/regulatory-considerations-human-cells-tissues-and-cellular-and-tissue-based-products-minimal (accessed on 4 September 2026).
147. European Medicines Agency. Advanced Therapy Medicinal Products: Overview. Available online: https://www.ema.europa.eu/en/human-regulatory-overview/advanced-therapy-medicinal-products-overview (accessed on 4 September 2026).
148. Regulation (EC) No 1394/2007 of the European Parliament and of the Council of 13 November 2007 on Advanced Therapy Medicinal Products and Amending Directive 2001/83/EC and Regulation (EC) No 726/2004. OJ L 324, 10.12.2007, pp. 121–137 (Consolidated Text of 26 July 2019). Available online: https://eur-lex.europa.eu/legal-content/EN/TXT/?uri=CELEX%3A32007R1394 (accessed on 4 September 2026).
149. Regulation (EU) 2017/745 of the European Parliament and of the Council of 5 April 2017 on Medical Devices. OJ L 117, 5.5.2017, pp. 1–175 (Consolidated Text of 1 January 2026). Available online: https://eur-lex.europa.eu/legal-content/EN/TXT/?uri=CELEX%3A32017R0745 (accessed on 4 September 2026). [PubMed]
150. European Medicines Agency. Advanced Therapy Classification. Available online: https://www.ema.europa.eu/en/human-regulatory-overview/marketing-authorisation/advanced-therapies-marketing-authorisation/advanced-therapy-classification (accessed on 4 September 2026).
151. Committee for Medicinal Products for Human Use and Committee for Advanced Therapies, European Medicines Agency. Reflection Paper on Classification of Advanced Therapy Medicinal Products. Available online: https://www.ema.europa.eu/en/documents/scientific-guideline/reflection-paper-classification-advanced-therapy-medicinal-products_en.pdf-0 (accessed on 4 September 2026).
152. Iglesias-López, C.; Agustí, A.; Obach, M.; Vallano, A. Regulatory Framework for Advanced Therapy Medicinal Products in Europe and United States. *Front. Pharmacol.* **2019**, *10*, 921. [CrossRef] [PubMed]
153. Vasanthan, K.S.; Kasturi, M.; Agarwal, P.; Seetharam, R.; Mathur, V.; Srinivasan, V. Innovative bioinks for 3D bioprinting: Exploring technological potential and regulatory challenges. *J. Tissue Eng.* **2025**, *16*, 20417314241308022. [CrossRef] [PubMed]
154. Tuftee, C.; Alsberg, E.; Ozbolat, I.T.; Rizwan, M. Emerging granular hydrogel bioinks to improve biological function in bioprinted constructs. *Trends Biotechnol.* **2024**, *42*, 339–352. [CrossRef] [PubMed]

155. Yu, J.; Yao, D.; Wang, L.; Xu, M. Machine Learning in Predicting and Optimizing Polymer Printability for 3D Bioprinting. *Polymers* **2025**, *17*, 1873. [CrossRef] [PubMed]
156. Xu, Y.; Sarah, R.; Habib, A.; Liu, Y.; Khoda, B. Constraint based Bayesian optimization of bioink precursor: A machine learning framework. *Biofabrication* **2024**, *16*, 045031. [CrossRef] [PubMed]
157. Vidler, C.; Halwes, M.; Kolesnik, K.; Segeritz, P.; Mail, M.; Barlow, A.J.; Koehl, E.M.; Ramakrishnan, A.; Aguilar, L.M.C.; Nisbet, D.R.; et al. Dynamic interface printing. *Nature* **2024**, *634*, 1096–1102. [CrossRef] [PubMed]
158. Hull, S.M.; Lou, J.; Lindsay, C.D.; Navarro, R.S.; Cai, B.; Brunel, L.G.; Westerfield, A.D.; Xia, Y.; Heilshorn, S.C. 3D bioprinting of dynamic hydrogel bioinks enabled by small molecule modulators. *Sci. Adv.* **2023**, *9*, eade7880. [CrossRef] [PubMed]
159. Machour, M.; Sider, R.; Szklanny, A.A.; Cohen, S.; Mishra, S.; Levenberg, S. Vascularized bone tissue engineering via 3D bioprinting: Recent progress and future perspectives. *Biomaterials* **2025**, *319*, 123406. [CrossRef] [PubMed]
160. Kim, B.S.; Cho, W.W.; Gao, G.; Ahn, M.; Kim, J.; Cho, D.W. Direct 3D printing of hierarchical vascular networks in cell-laden constructs. *Biomater. Adv.* **2024**, *158*, 213770. [CrossRef] [PubMed]

Disclaimer/Publisher's Note: The statements, opinions and data contained in all publications are solely those of the individual author(s) and contributor(s) and not of MDPI and/or the editor(s). MDPI and/or the editor(s) disclaim responsibility for any injury to people or property resulting from any ideas, methods, instructions or products referred to in the content.